Advanced Drug Delivery Reviews 175 (2021) 113798

Contents lists available at ScienceDirect

Advanced Drug Delivery Reviews

journal homepage: www.elsevier.com/locate/adr

Tumor-on-chip modeling of organ-specific cancer and metastasis

Nuala Del Piccolo [a], Venktesh S. Shirure [a], Ye Bi [d], S. Peter Goedegebuure [d], Sepideh Gholami [b], Christopher C.W. Hughes [c], Ryan C. Fields [d], Steven C. George [a,*]

[a] Department of Biomedical Engineering, University of California, Davis, One Shields Ave, Davis, CA 95616, United States
[b] Department of Surgery, University of California, Davis, 2335 Stockton Boulevard, Sacramento, CA 95817, United States
[c] Department of Molecular Biology & Biochemistry and Department of Biomedical Engineering, University of California, Irvine, CA 92697-3900, United States
[d] Department of Surgery, The Alvin J. Siteman Cancer Center, Washington University School of Medicine, 660 S. Euclid Ave, St. Louis, MO 63110-1010, United States

ARTICLE INFO

Article history:
Received 27 February 2021
Revised 4 May 2021
Accepted 11 May 2021
Available online 18 May 2021

Keywords:
Tumor microenvironment
Metastatic niche
Tissue engineering
Organ-on-chip
Microfluidic model
Microphysiological system

ABSTRACT

Every year, cancer claims millions of lives around the globe. Unfortunately, model systems that accurately mimic human oncology – a requirement for the development of more effective therapies for these patients – remain elusive. Tumor development is an organ-specific process that involves modification of existing tissue features, recruitment of other cell types, and eventual metastasis to distant organs. Recently, tissue engineered microfluidic devices have emerged as a powerful *in vitro* tool to model human physiology and pathology with organ-specificity. These organ-on-chip platforms consist of cells cultured in 3D hydrogels and offer precise control over geometry, biological components, and physiochemical properties. Here, we review progress towards organ-specific microfluidic models of the primary and metastatic tumor microenvironments. Despite the field's infancy, these tumor-on-chip models have enabled discoveries about cancer immunobiology and response to therapy. Future work should focus on the development of autologous or multi-organ systems and inclusion of the immune system.

Contents

Abbreviations: TME, tumor microenvironment; CAF, cancer-associated fibroblast; ECM, extracellular matrix; CSC, cancer stem cell; TAM, tumor-associated macrophage; MDSC, myeloid-derived suppressor cell; NK cell, natural killer cell; Treg, regulatory T cell; EMT, epithelial mesenchymal transition; MET, mesenchymal-epithelial transition; EC, endothelial cell; PBMC, peripheral blood mononuclear cell; CTC, circulating tumor cell; VEGF, vascular endothelial growth factor; IL, interleukin; MMP, matrix metalloproteinase; FGF, fibroblast growth factor; TGFβ, transforming growth factor β; TNF, tumor necrosis factor; SCLC, small cell lung cancer; NSCLC, non-small cell lung cancer; BC, breast cancer; DCIS, ductal carcinoma in situ; PCa, prostate cancer; AR, androgen receptor; CRC, colorectal cancer; MSS, microsatellite stable; MSI-H, microsatellite instability-high; PDAC, pancreatic ductal adenocarcinoma; UV, ultraviolet; LSEC, liver sinusoidal endothelial cell; HSC, hematopoietic stem cell; MSC, mesenchymal stem/stromal cell; BBB, blood-brain barrier; BTB, blood-tumor barrier.

* Corresponding author.
E-mail address: scgeorge@ucdavis.edu (S.C. George).

https://doi.org/10.1016/j.addr.2021.05.008
0169-409X/

1. Introduction

In 2020 alone, there were an estimated 19.3 million new cancer cases and 9.9 million cancer-related deaths around the world [1–4], highlighting the tremendous impact this devastating disease has on human quality of life and global economics. Cancer develops when human cells acquire the capacity for uncontrolled growth, usually at the expense of normal host physiology [2,4–6]. Metastasis—a common step in tumor progression—occurs when cell(s) from a primary tumor gain migratory phenotypes, enter the blood or lymph vessels, travel to a distant site, exit the vessel network, and establish a new colony of cancer cells (i.e., a tumor) [5–7]. Though primary tumors are the bulk of diagnosed cases, metastatic cancer accounts for the majority (~90%) of deaths [8,9].

The hallmark attributes of a tumor lesion, as detailed in a pair of seminal papers by Douglas Hanahan and Robert Weinberg [5,6], include rapidly proliferating tumor cells, cancer-associated fibroblasts (CAFs), immune cells, a remodeled extracellular matrix (ECM), angiogenesis, high interstitial pressure, gradients of soluble factors, and hypoxia. As a tumor develops, it adapts and modifies the unique characteristics of the affected organ—for example, the architecture, specialized cell types, vascular and lymphatic networks, oxygen tension, and ECM composition—to support tumor growth [5–12]. Together, this heterogeneous and dynamic collection of structures, cells, and physiochemical factors is known as the tumor microenvironment (TME) (Fig. 1). Recent work demonstrates that the TME is a primary driver of tumor progression and a potential therapeutic target [5,12–14].

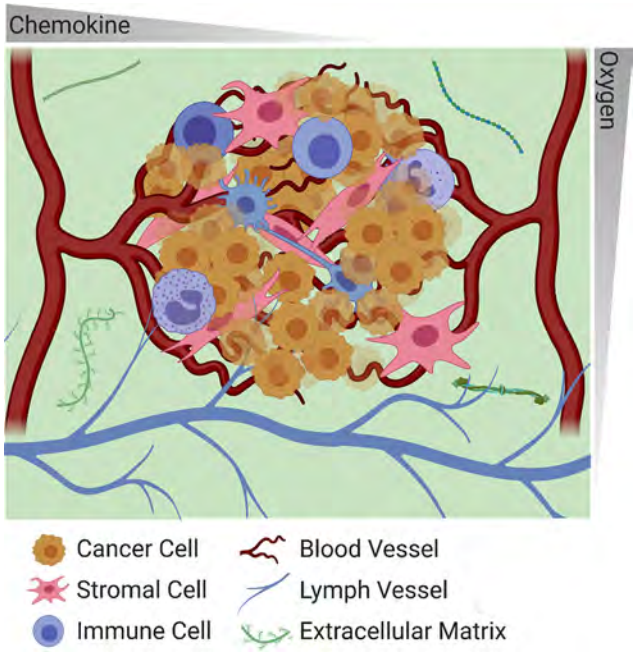

Fig. 1. Primary tumor microenvironment. This cartoon rendition of a generalized tumor microenvironment depicts typical features of the TME, including: tumor cells (yellow), fibroblasts (pink), immune cells (purple), an abnormal vasculature (red) adjacent to lymphatic vessels (blue), a remodeled extracellular matrix (green), and oxygen and chemokine gradients (gray). (For interpretation of the references to colour in this figure legend, the reader is referred to the web version of this article.)

Tumor cells can spread from the primary affected organ to a distant site through a multi-step process known as the metastatic cascade (Fig. 2). This process begins in the primary tumor, with the secretion of exosomes and soluble factors into the bloodstream. These signals travel to common metastatic sites, where they are thought to prime the tissues to support new tumor lesions. Next, primary tumor cells gain invasive and migratory phenotypes through an epithelial-mesenchymal transition (EMT). These cells can then intravasate across the endothelial barrier of blood and lymph vessels and travel through the body as circulating tumor cells (CTCs). CTCs that survive in the circulation can extravasate back across the endothelium of a vessel into a second organ—often the lung, liver, bone, or brain [5–7]. After extravasating into the new organ, CTCs undergo a mesenchymal-epithelial transition (MET), which promotes survival in the tissue parenchyma [7,15]. Cells may also survive in a semi-dormant state before remodeling occurs [15]. Two early competing hypotheses described the selection of a metastatic site: Stephen Paget's 1889 "seed and soil" hypothesis argued that CTCs survive and grow in distant organs that provide a favorable environment [16]; and James Ewing's 1928 "mechanical hypothesis" stated that mechanical mechanisms entrap CTCs at specific locations [17]. A third emerging hypothesis contends that CTCs that survive initial seeding in a distant organ either act alone or, more likely, interact with local stromal cells and/or infiltrating macrophages to create a supportive TME [18,19].

Current standard-of-care for cancer patients includes surgery, chemotherapy, and radiation; immunotherapies are emerging as an exciting new option [2–6]. Though historical identification and development of these treatments has hugely improved the prognosis of newly diagnosed cancer patients, the current pipeline for new oncology therapies is relatively stagnant, with only 3–5% of anti-cancer agents entering clinical trials ultimately receiving FDA approval [20,21]. This is partly attributed to the limitations of current preclinical model systems—namely, 2D cell culture, static spheroid/organoid culture, and murine models—which struggle to recreate the unique geometry, composition, and physiochemical properties of the human TME [21,22].

Recently, organ-on-chip models have emerged as a powerful tool for the study of human physiology and pathology at the molecular, cellular, and tissue levels. To create these models, researchers pattern 3D channels and chambers into polydimethylsiloxane or other flexible polymers using soft lithography or 3D printers. The channels and chambers are filled with hydrogels containing cells or perfused with fluid to mimic the architecture and mechanical forces of human tissue. Notably, these models offer a physical scale (tens to hundreds of micrometers) that matches that of the TME; a modular design that enables selection of cells and ECM; and precise control of physiochemical properties like interstitial pressure, soluble factor gradients, and oxygen tension. Further, events in organ-on-chip platforms can be monitored with high spatiotemporal resolution using microscopy. However, as an emerging technology, organ-on-chip models lack standardization, can be technically challenging to create, and have suffered from limited reproducibility and throughput [21,23].

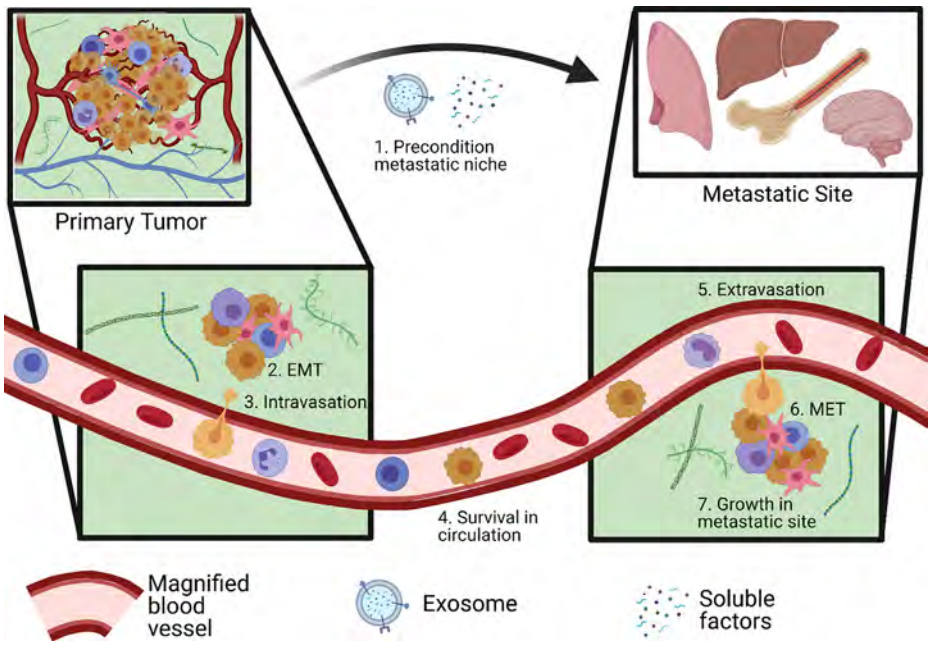

Fig. 2. The metastatic cascade. Metastasis from the primary tumor to a distant organ is a multi-step process that takes place through the blood or lymph vessels (this cartoon depicts the former). (1) The primary tumor releases exosomes and soluble factors that travel to the metastatic site and condition the organ to support metastasis. (2) Primary tumor cells undergo epithelial-to-mesenchymal transitions (EMT), a change that is marked by invasive and migratory phenotypes. (3) These tumor cells intravasate into the vessel network and (4) travel through the body as circulating tumor cells (CTCs). (5) CTCs that survive in the circulation and arrive in the target metastatic organ can extravasate into the organ parenchyma. (6) Tumor cells in the organ parenchyma revert to their original characteristics through the mesenchymal-epithelial transition (MET). (7) These tumor cells then survive and grow to form a metastatic lesion.

Numerous recent review papers examine the utility of microfluidic models to study specific features of the TME [21,24–33]. Here, we offer an organ-specific perspective on microfluidic models of the primary and metastatic TME. We focus our attention on organs with the highest annual cancer burden (broadly interpreted as incidence plus deaths). These primary tumors are found in the lung, breast, prostate, colon/rectum, pancreas, and skin. The most common metastatic sites are the lung, liver, bone, and brain [2–4]. First, we describe the normal anatomy and physiology of each organ. Next, we identify the unique features of each tumor lesion, with a focus on properties that can be modeled using microfluidic technologies. Then, we summarize current progress modeling each organ-specific TME using organ-on-chip platforms. Finally, we discuss gaps in the literature that would improve the organ specificity of existing models.

2. Primary Tumors

2.1. Lung Cancer

Relevant Anatomy and Physiology. While the primary function of the lungs is respiratory gas exchange (oxygen and carbon dioxide), the lungs also have important roles in host defense, acid-base balance, metabolism, and phonation [34–37]. Respiratory gas exchange occurs almost exclusively in the delicate alveolar tissue that is comprised of "grape-like" clusters of small air-filled sacs called alveoli (diameter 50–100 μm). The alveoli are located at the endpoints of bronchi, the branching airways that function as a conduit for air to travel from the outside environment, through the trachea, into the alveolar region, and vice versa [34,35]. The bronchi are supplied by a network of blood vessels—the bronchial circulation—which is derived from the left side of the heart and serves to provide nutrients and remove waste products from the airway tissue [36]. The alveoli have a very thin membrane (0.5 μm) that separates the air from the blood in the pulmonary circulation. The alveolar membrane consists of type I and type II epithelial cells, endothelial cells (ECs), and fibroblasts, and is characterized by two major and somewhat unique features: 1) an air-tissue interface; and 2) cyclical mechanical strain during breathing [35]. In addition to the cells that comprise the alveolar membrane, the alveoli also contain leukocytes (predominantly macrophages) that participate in the innate immune response to inhaled foreign particles [37]. Blood circulation through the alveoli is derived from the right side of the heart, which represents the entire cardiac output [36]. An ideal model of the alveolar region of the lung would recreate its spherical geometry; include a dynamic model of the pulmonary circulation and interstitial space; incorporate epithelial, stromal, and immune cells; and be subject to cyclic strain at the magnitude and frequency which matches *in vivo* conditions.

Primary Lung Cancer. Many outstanding reviews describe the basic features (categorization, staging, and treatment) of lung cancer [12,38]; herein, we will summarize these fundamental features (Fig. 3A, Table 1), with a focus on those that can potentially be recreated in a microfluidic model. Lung cancer is the most common cause of cancer-related deaths worldwide and can be broadly broken into two major categories: i) small cell lung cancer (SCLC, 10–15% of all lung cancer); and ii) non-small cell lung cancer (NSCLC, 80–85% of all lung cancer); rare lung cancers comprise the balance of cases. NSCLC can be further broken down into squamous cell lung cancer (25–35% of all lung cancer), lung adenocarcinoma (40% of all lung cancer), and large cell carcinoma (10% of all lung cancer) [38,39]. The specific cellular source for lung cancer remains an active area of research and debate. The current consensus suggests that SCLC arise from the neuroendocrine cells in the lung, while NSCLC arise from the type II alveolar epithelial cell (adenocarcinoma) or basal epithelial cells in the larger airways (squamous cell lung cancer). Generally, lung cancers are highly mutated [39], and therefore respond well to immunotherapy. Additional features of the tumor microenvironment present in NSCLC include regions

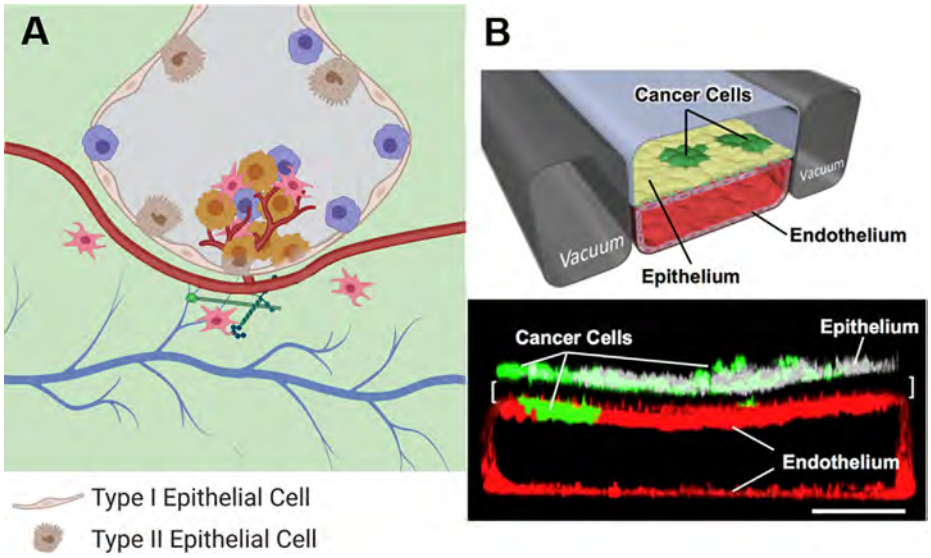

Fig. 3. Primary lung TME. (A) Lung tumors originate in highly mutated cells lining the alveoli, or air-filled sacs surrounded by blood vessels. The lung TME is characterized by the presence of immunosuppressive TAMs, MDSCs, and dendritic cells; a stiff ECM composed of laminin, collagen IV, proteoglycans, and hyaluronan; and angiogenesis. (B) The Ingber lab developed a lung-on-chip model [58]. Epithelial (yellow) and endothelial (red) cells were cultured on opposite sides of a flexible, porous membrane dividing a chamber into an air channel (upper) and fluid channel (lower); this design replicated the air-tissue interface of the alveoli. Application of vacuum pressure in the adjacent fluidic lines generated the cyclic mechanical stress of breathing. NSCLC cells (green) were introduced on the epithelial side of the membrane. (For interpretation of the references to colour in this figure legend, the reader is referred to the web version of this article.)

Table 1
A summary of the organ-specific features of common primary tumors.

Primary Tumor	Prominent Features
Lung	• Highly mutated tumor cells • Air-tissue interface • Abundant immune cell infiltrate characterized by TAMs, MDSCs, and dendritic cells • Stiff ECM rich in laminin, collagen IV, proteoglycans, and hyaluronan • Large CAF population • Angiogenesis
Breast	• Tumor cells are classified by expression of 3 hormone receptors (progesterone receptor, estrogen receptor, human epidermal growth factor receptor 2) • Loss of myoepithelial cells • Recruitment of macrophages and T cells • Dense and stiff ECM characterized by aligned collagen fibers • Large CAF population • Hypoxia
Prostate	• Tumor cells have few mutations, are clonally distinct, and depend on androgen receptor signaling • Paucity of immune cells, immunosuppression • Stiff ECM rich in collagen I and tenascin-C, remodeled by MMPs and loss of laminin • Large CAF population • Angiogenesis
Colon/rectum	• Tumor cells originate in multipotent stem cells found at the base of crypts • MSI-H tumors: highly mutated, proinflammatory immune cell infiltrate • MSS tumors: chromosomal abnormalities, immunosuppressive immune cell infiltrate • Large CAF population • Microbiome
Pancreas (PDAC)	• Tumor cells have few mutations • Abundant immune cell infiltrate characterized by TAMs, Tregs, and MDSCs • Dense and stiff ECM rich in collagens, hyaluronic acid, and glycoproteins • Large CAF population • High interstitial pressure • Hypovascularization, hypoxia
Skin (melanoma)	• UV damage produces highly mutated tumor cells • Air-tissue interface • Large population of immune cells includes TAMs, neutrophils, NK cells, dendritic cells, and cytotoxic T cells • Remodeled ECM comprised of collagen, fibronectin, & laminin • Angiogenesis

of hypoxia, angiogenesis induced by tumor and immune cell expression of vascular endothelial growth factor (VEGF) [12,40], a large population of CAFs, and immune cells. CAFs in the lung TME support the survival and growth of tumor cells and cancer stem cells (CSCs) through secretion of chemokines like interleukin (IL)-6 and insulin-like growth factor 2 and promote immunosuppression through expression of programmed cell death receptors and ligands [12]. The immune infiltrate is dominated by immunosuppressive myeloid-derived suppressor cells (MDSCs) and tumor-associated macrophages (TAMs) [12,38], but also includes proin-

flammatory B and T cells [12] and lymphoid structures that contain mature and follicular dendritic cells [41]. In addition to the cells present in the lung tumor microenvironment, the ECM of lung cancer is altered and plays an important role in progression and survival; salient features include enhanced expression of basement membrane proteins such as laminin and collagen IV, an ECM that is stiffer compared to normal lung stroma, and altered expression of proteoglycans and hyaluronan [12,42]. The features of the lung TME have been shown to impact tumor and immune cell migration and patient prognosis.

Microfluidic Models of Lung Cancer. While *in vitro* models of lung biology and lung cancer have been around for decades, these have largely been limited to monolayer culture of lung epithelial cells or planar 3D tissue models with air–liquid interfaces [43,44]. Modeling lung biology and physiology using microfluidic devices began with a seminal report in 2010, in which a monolayer of epithelial cells and ECs were cultured on opposite sides of a flexible membrane [45]. The model was able to capture both the dynamic mechanical strain present in the alveolar region and an air–liquid interface (Fig. 3B). The model was then used to investigate impactful problems related to immune cell trafficking and drug treatments [45–47]. Together, these studies paved the way for microfluidic models that captured important features of lung cancer, including the airways and the vasculature.

The vast majority of microfluidic models of lung cancer have used cell lines derived from NSCLC, with the A549 cell line used most frequently [48–57]. A549 cells grow as a monolayer in 2D cultures and a spheroid in 3D culture. These cells have been used for decades in 2D monolayer cultures to model features of normal lung biology, the type II pneumocyte, and lung cancer, so there is a wealth of data to compare between microfluidic and traditional *in vitro* assays. When cultured in microfluidic devices, A549 cells typically adopt the spheroid morphology—due to their inability to form intercellular junctions—and these platforms have been used to investigate a range of important questions. For example, a microfluidic device has been used to generate spatial gradients in growth factors from neighboring stromal cells to understand fundamental mechanisms related to drug resistance in lung cancer [49]. Additionally, A549 spheroids cultured in microfluidic devices have been used to study the efficiency of photodynamic therapy [50]. Microfluidic devices have also been used to separate distinct cell types present in lung cancer such as CAFs and ECs [51,55], enabling precise control and characterization of cell–cell communication in the lung cancer TME. Multiple studies cultured NSCLC cell lines (namely, A549 or H1975 cell lines) in microfluidic models in order to examine the role of mechanical forces present in the lung—including fluid flow in the interstitium [54] and blood [51,55], and mechanical stretch (Fig. 3B) [58]—on tumor progression and drug response. NSCLC cells (H560 cell line) cultured in microfluidic models have also been used to investigate communication between a lung tumor and bacteria [59].

Though more limited, several recent studies have demonstrated the ability to culture primary lung cancer as organoids in microfluidic devices [53,60,61]. For example, Li and colleagues isolated CAFs from patients with lung adenocarcinoma and investigated their impact on tumor cell (A549) migration [53]. A pair of studies from the Borenstein group cultured small primary tumor organoids from NSCLC patient tumor biopsies with autologous tumor infiltrating lymphocytes under dynamic perfusion, enabling characterization of tumor-immune interactions [61] and prediction of patient-specific response to immune checkpoint blockade therapies [60]. The latter two studies are particularly exciting as they demonstrate the capacity to probe patient-specific tumor immunobiology and drug responses.

Future Directions. Microfluidic models of lung cancer should carefully consider the tumor cell class (e.g., SCLC or NSCLC) and source (e.g., cell line or primary); the inclusion of additional cell types, such as ECs, CAFs, and/or immune cells; the source of proteins to model the ECM; and hypoxia. Further, the role of immune cell phenotype and infiltration, ECM composition, and mechanical strain on lung cancer biology and response to therapy remain incompletely characterized.

2.2. Breast Cancer

Relevant Anatomy and Physiology. The breast is a gland located on the chest; in females, its primary function is to produce milk for offspring. The gland is responsive to the hormones estrogen, progesterone, and prolactin, which aid in gland development during puberty and pregnancy [62,63]. Each mammary gland consists of 15–20 lobes, where each lobe is a group of 20–40 functional units known as terminal ductal lobular units (or, lobules). The lobules (1–4 mm) are clusters of 10–100 tiny sack-like acini (~100 μm) [62]. Acini are hollow structures with an inner lining of milk-producing epithelial cells surrounded by a layer of myoepithelial cells and enclosed in a protective basement membrane. The basal myoepithelial cells generate contractile force to eject milk from the lumen of the acini into collecting ducts, and a network of ducts carries the milk from the lobules to the nipple [10,62,64]. The lobes of the mammary gland are situated in connective tissue comprised of ECM rich in laminin and collagen; containing adipocytes and fibroblasts; and interlaced with lymphatic and blood vessels [10,63,64].

Primary Breast Cancer. Breast cancers (BCs) (Fig. 4A, Table 1) are classified into two broad categories based on their cellular origin: carcinomas originate from epithelial cells lining ducts or lobules and account for ~ 95% of all BCs, while sarcomas arise from ECs or myofibroblasts and comprise < 1% of all BCs. Ductal carcinoma in situ (DCIS) tumors remain restricted to the luminal structures and account for ~ 15% of all newly diagnosed carcinomas. The remaining 85% of carcinomas are invasive; that is, they have breached the connective tissue and entered the surrounding fatty tissue, have lost the basement membrane and myoepithelial cells found in healthy lobules, and possess a significant potential to enter the lymphatics or blood vessels and metastasize to different organs [10,65]. BC is also classified based on the presence or absence of hormone receptors—namely, the progesterone receptor, estrogen receptor, and human epidermal growth factor receptor 2. Tumors lacking all three receptors—known as triple-negative BC—exhibit basal-like molecular subtyping, more aggressive biologic behavior, poorer patient prognoses, and resistance to standard chemotherapy regimens [65].

Following activation by soluble factors released by tumor cells, CAFs and TAMs remodel the ECM found in healthy breast tissue to generate the distinctively dense and stiff ECM found in the BC TME. This process is marked by deposition of collagen I, matrix metalloproteinases (MMPs), and tissue inhibitors of metalloproteinases, followed by crosslinking and alignment of collagen fibers [10,64,66,67]. Since tumor cells migrate along aligned collagen fibers, the remodeled ECM promotes tumor invasion and metastasis. In fact, alignment of collagen fibers perpendicular to the TME correlates with worse patient prognoses [68]. The stiffness of the ECM found in BC tumors also compresses blood vessels, leading to hypoxia [67]; alters gene expression in epithelial and stromal cells to promote tumor progression and resistance to therapy [10,66]; generates regions of highly concentrated cytokines [66,67]; and increases integrin clustering and signaling in tumor cells, enabling invasive phenotypes [66,67]. The BC TME is also marked by loss of tumor-suppressive myoepithelial cells [10,64] and hypoxia (partial pressure of oxygen of 10 mm Hg). Hypoxia and subsequent HIF-1α expression in BC tumors promote angiogenesis and tumor cell growth, motility, EMT, and metastasis to

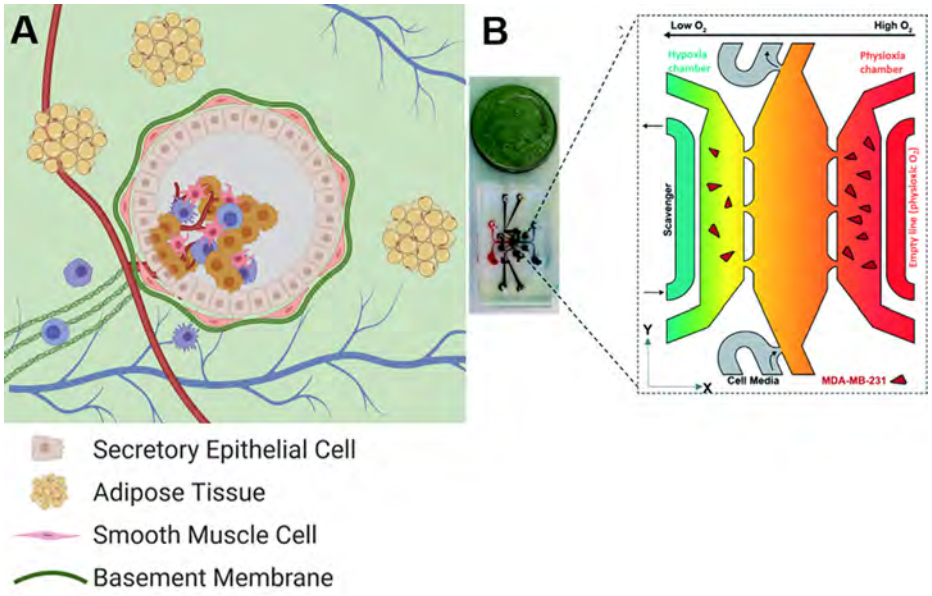

Fig. 4. Primary breast TME. (A) Breast cancers arise in the milk-producing epithelial cells found in acini and are classified by their expression of 3 hormone receptors (progesterone receptor, estrogen receptor, and human epidermal growth factor receptor 2 hormone). The BC TME is characterized by recruitment of macrophages and T cells; a large CAF population; a dense, stiff ECM marked by aligned collagen fibers; and hypoxia. (B) Our lab reported a microfluidic device that enables precise spatiotemporal control of oxygen device in a hydrogel. We used the platform to study the effects of hypoxia on the BC cell line MDA-MB-231 [78]. Reproduced from Ref. 78 with permission from The Royal Society of Chemistry.

neighboring lymph nodes. Hypoxia in the TME is also linked to expression of enzymes that crosslink and organize collagen, further stiffening the ECM [69].

Microfluidic Models of Breast Cancer. The unique features of the breast tissue—including acini structure, matrix stiffness, and immune and stromal cell populations—play a critical role in BC development and progression. Since microphysiological systems offer facile control over these architectural and environmental features, they represent a potent tool for the study of carcinomas and sarcomas in breast tissue. For example, a recent report recreated the structure of acini by coating normal mammary ductal epithelial cells and a collagen hydrogel seeded with randomly distributed mammary fibroblasts on either side of a semipermeable, ECM-coated membrane representing the basement membrane. DCIS cell spheroids introduced on the epithelial side of the membrane integrated with the epithelium, did not invade the stromal layer, and were sensitive to the chemotherapy paclitaxel (normal mammary epithelial cells showed no chemotoxicity) [70]. In another microfluidic model of DCIS, a hollow conduit lined with mammary epithelial cells was patterned into a collagen hydrogel containing mammary fibroblasts [71,72]. DCIS cells introduced into the lumen increased hypoxia throughout the microphysiological model; relied on both enhanced glucose metabolism and glycolysis; and were selectively targeted by the chemotherapy doxorubicin [72]. Additionally, paracrine signaling from fibroblasts induced DCIS cells to breach the epithelial wall, providing insight into how in situ tumors evolve towards invasive ductal carcinoma [71].

Microfluidic models that incorporate the microvasculature—either through patterning techniques [73,74] or self-organization of ECs [75,76]—enable study of angiogenesis and intravasation in the BC TME. For example, Zervantonakis et al. [73] examined intravasation in a device where an ECM-filled chamber separated an EC-lined channel from a chamber filled with BC cells in a hydrogel. Macrophages in the lumen of the vessel-mimetic chamber secreted tumor necrosis factor (TNF)-α, which increased both the permeability of the endothelial barrier and BC cell intravasation into the chamber. A similar study introduced natural killer (NK) cells into EC-lined channels on either side of a hydrogel containing BC spheroids. The NK cells migrated towards and penetrated the spheroids, where they killed tumor cells; NK cytotoxicity was enhanced by cancer-targeted antibodies, replicating antibody-dependent cell cytotoxicity [77]. In a 2018 study by our group, ECs and normal fibroblasts were combined to generate self-assembled microvascular networks in the central chamber of a device. Then, patient-derived BC tumor organoids were introduced into adjacent chambers; the BC cells induced angiogenesis from the quiescent vascular network into the tumor chamber and intravasated into the capillary lumens. We also delivered chemotherapies to the tumor organoids through the vascular network and observed reductions in both angiogenesis and tumor growth, demonstrating the utility of the platform for personalized medicine applications [75].

Additional microfluidic models mimic the unique features of the BC TME, including hypoxia [78,79] and tumor-stromal cell interactions [80–83]. Recently, our group established a spatiotemporal method to precisely control oxygen tension in a microfluidic device [79]. We applied the technique to show that even mild hypoxic conditions (oxygen tension < 4%) increase the proliferation and migration of MDA-MB-231 BC cells in fibrin gels and that these phenotypes depend on HIF-1α expression (Fig. 4B) [78]. Truong and colleagues cultured the BC cell line SUM-159 in a circular chamber adjacent to a concentric chamber; the chambers were filled with hydrogels comprised of Matrigel, collagen, or a mix of the two. In this device, the research team showed that when the concentric chamber contained i) an EGF gradient [83] or ii) patient-derived CAFs [82], BC cells migrated towards and invaded the outer chamber. Morgan et al. [81] explored estrogen signaling in an organotypic microfluidic model comprised of a MCF7 BC cell-lined lumen in a hydrogel embedded with fibroblasts. The results show that 17-β estradiol increases MCF7 proliferation and that fibroblasts moderately enhance this effect. Further, the team incorporated patient-derived stromal cells into the system and examined the efficacy of therapies that inhibit estrogen signaling. They found that inhibiting the enzyme aromatase—which is expressed in stromal cells and metabolizes testosterone to estrogen—is more effective in stromal cells from lean than obese patients. In addition

to shedding light on the moderate efficacy of aromatase inhibitors, the results highlight the utility of the platform for personalized medicine [80].

Future Directions. Current microfluidic models accurately recreate the architecture of breast tissue and separately incorporate CAFs, immune cells, or hypoxia. However, a comprehensive platform remains elusive, and only a few model systems use primary cell sources. Additionally, the technology used to model blood vessels in the TME should be adapted to model lymphatic vessels, a key feature of both breast tissue anatomy and BC metastasis. Further, microfluidic models have the potential to more fully elucidate the role of hormone signaling in BC development, progression, and response to therapy.

2.3. Prostate Cancer

Relevant Anatomy and Physiology. The male prostate is a walnut-sized gland located at the base of the bladder and in front of the rectum; its primary function is to secrete alkaline fluids that protect and nourish sperm [84–86]. The gland is encased in fibromuscular tissue, bisected by the urethra, and composed of many interconnected acini. The urethra is a tube through which urine and sperm flow, and the fibromuscular tissue surrounding the gland—composed of smooth muscle and collagen—facilitates fluid flow to and through the urethra [84]. Acini in the prostate are hollow spheres with three concentric layers: an outer basement membrane, a basal cell barrier, and an inner lining of secretory cells. The basal cell barrier separates the basement membrane from the secretory cells—a structure typical of glandular organs—and is also dotted with a handful of neuroendocrine cells, which support the growth of secretory cells through paracrine signaling. The innermost secretory luminal cells are dependent on the hormone androgen to produce and release specialized fluids into the core of the acini; these fluids then pass through a network of ducts to the urethra, where they protect and nourish sperm during ejaculation [85]. The prostate gland can be classified into three morphological zones—the transition zone, the central zone, and the proximal zone—each of which is linked to specific diseases [85,86] and loosely interlaced with smooth muscle tissue [84]. The proximal zone accounts for the majority of the gland (70% volume), is located towards the base and along the outside of the gland, and gives rise to the majority of prostate cancers [84,85].

Primary Prostate Cancer. Prostate cancer (PCa) (Fig. 5A, Table 1) is the second most commonly diagnosed cancer in males. The majority of PCas are adenocarcinomas that originate in secretory cells found in the proximal zone. PCas can also form in neuroendocrine cells, and these tumors are particularly aggressive [84,85]. The development of adenocarcinomas in the prostate begins with uncontrolled growth of secretory cells in the acinar core and loss of basal cells; the disease is considered invasive when the basement membrane surrounding the acini is broken [85]. PCas are uniquely heterogeneous and tumor cells in adjacent acini are often clonally distinct [85]. Additionally, these tumor cells are relatively slow growing, display chromosomal abnormalities (mostly allelic losses), and demonstrate aberrant androgen receptor (AR) and phosphoinositide 3-kinase signaling [11,85,87].

Aberrant AR signaling is a hallmark of PCa and a frequent therapeutic target [85,87–89]. AR is a transcription factor that increases cellular growth and proliferation following binding of agonists like testosterone and 5α-dihydrotestosterone. In PCa, AR signaling is upregulated through overexpression of AR or its coactivators, mutations in the binding pocket of AR that expand the ligands it recognizes, or ligand-independent AR activation [88,89]. Therapies that block AR signaling—including removal of the testosterone-producing testes and treatment with AR antagonists—are effective in early-stage cancers, but often lead to the development of androgen-independent tumors, which are associated with invasive tumor cell phenotypes, metastasis, and poor patient prognosis [88,89].

Crosstalk between stromal cells and cancer cells is a driving force for carcinogenesis in the prostate [11,85,90,91]. The stromal cell population in the PCa TME is larger than and activated compared to that found in healthy prostate tissue. These cells are involved in ECM remodeling—specifically, loss of laminin, deposition of collagen I and tenascin-C, and secretion of proteases including MMPs—and these changes increase matrix stiffness and promote tumor cell proliferation, migration, and metastasis [90–92]. Enhanced fibroblast growth factor (FGF), Src, and VEGF signaling by stromal cells in the PCa TME promotes neovascularization of the tumor [11,90]. The stroma also contributes to dysregulation of the transforming growth factor β (TGFβ) pathway, which is involved in ECM deposition, immune cell modulation, and tumor cell proliferation and resistance to AR therapy [11].

PCa also demonstrates a unique immunosuppressive TME [87,91]. Tumor cells have a low mutational burden, often retain

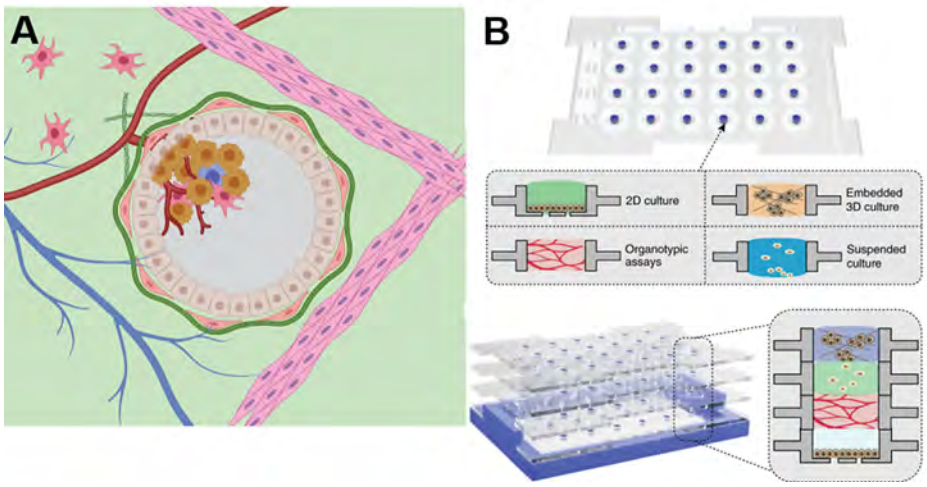

Fig. 5. Primary prostate TME. (A) Prostate cancers develop in secretory cells in acini, have a low mutational burden, and depend on androgen receptor signaling. The PCa TME is characterized by an immunosuppressive environment largely devoid of immune cells; an abundant CAF population; and a stiff ECM rich in collagen I and tenascin-C. (B) The PCa TME was modeled using a modular microfluidic device composed of separate chambers containing tumor cells, monocytes, and vascular networks [96]. As pictured here, these chambers can be stacked and analyzed with precise temporal control.

the cellular machinery necessary for genetic repair, and downregulate expression of major histocompatibility complex I and phosphatase and tensin homolog deleted on chromosome ten (the former enables T cell recognition of cancer cells, the latter is involved in recruitment of immunosuppressive cells) [87]. TAMs, MDSCs, and regulatory T cells (Tregs) in the PCa TME may support tumor growth and progression [87,91]. In contrast to patterns observed in other tumors, high T cell infiltration into the PCa TME correlates with poor patient prognosis. An explanation for this effect remains undetermined, though it may be linked to aberrant T cell function—for example, suppression or exhaustion—induced by the TME [87].

Microfluidic Models of Prostate Cancer. Jiang and colleagues reported a microfluidic model of a healthy prostate gland, which features perfusion coculture of prostate stromal and basal cells on opposite sides of a flexible, porous membrane. This model simulates paracrine communication between the cells types, exemplified by the differentiation of basal cells to secretory cells through an AR-mediated mechanism [93]. Additionally, microfluidic models of the PCa TME have sought to mimic stromal-tumor cell crosstalk [94], simulate immunity [95,96], and test chemotherapeutic drugs [97,98]. To mimic a prostate duct in a microfluidic device, Kerr and colleagues cultured epithelial cells in a lumen surrounded by matrix-embedded fibroblasts; the cells were selected to represent various stages of PCa progression. Peripheral blood mononuclear cells (PBMCs) cultured in the lumen of metastatic TME models demonstrated a higher redox ratio—a state linked to immunosuppression—and increased expression of genes associated with angiogenesis, tumor cell proliferation and migration, and pro-tumor processes than PBMCs in primary TME models [95]. A 2019 report outlined a microfluidic device comprised of stackable layers of chambers; this platform offers unique temporal control over microtissue contact and analysis (Fig. 5B). As proof-of-concept, the study explored the impact of androgen-dependent and -independent PCa cells on macrophage phenotype and function. The results showed that androgen-independent PCa cells differentiated macrophages towards immunosuppressive phenotypes, which support angiogenesis; in contrast, androgen-dependent PCa cells fostered pro-inflammatory macrophage phenotypes and blood vessel networks characterized by short branches [96]. Further, Pandya et al. [97] combined perfused 3D culture of tumor cells (including PCa) and electrical sensing in a microfluidic device to rapidly screen the efficacy of chemotherapies. Lin et al. [98] created a concentration gradient of the therapy docetaxel in a microfluidic device to characterize the relationship between this condition and the development of PCa resistance to therapy. Another study showed that paracrine hedgehog signaling from stromal cells supports tumor cell growth through culture of stromal and tumor cells in separate chambers of a microfluidic device [94].

Future Directions. Despite the prominent role of AR signaling on PCa development, microfluidic models recapitulating this feature—and the subsequent development of resistance to AR-directed therapies—are currently limited. Adding this feature to the current morphologically accurate models of primary and metastatic PCa acini and ducts may produce useful insight into patient prognosis and response to therapy. Additionally, incorporating multiple immune cell lineages into future models may help answer open questions about immunosuppression—especially the unusual function of T cells—in the PCa TME. A complete model of the TME should also include the ECM composition and stromal cell populations typical of PCa.

2.4. Colorectal Cancer

Relevant Anatomy and Physiology. The colon, also known as the large intestine, is the final section of the digestive system. It is a folded organ that is approximately 5 feet long and narrows from start to end. It is located directly after the small intestine and consists of six anatomically consecutive parts: the cecum; the ascending, transverse, descending, and sigmoid colon; and the rectum. The primary functions of the colon are to absorb water and electrolytes from digested food, absorb and produce vitamins, and pass increasingly solidified waste forward. The rectum stores feces prior to defecation [99–101].

The wall of the colon consists of five layers. From the lumen out, these are: the mucosa, the submucosa, the muscularis propria, the subserosa, and the serosa [101]. The mucosa consists of a single layer of epithelial cells arranged into long narrow invaginations (or crypts). There are two types of epithelial cells: absorptive cells and secretory luminal cells. The latter produces a thick mucus layer that covers the mucosa, facilitating movement of waste through the colon [99]. Commensal bacteria in the lumen of the colon produce vitamins, degrade insoluble fibers like cellulose, and maintain homeostasis in the colon [99,100,102]. The submucosa is a subepithelial layer of connective tissue and lymph nodes. The muscularis propria is a thick layer of smooth muscle cells that rhythmically contract to generate peristalsis and move waste forward through the colon [99]. The subserosa and serosa are thin layers of fat and connective tissue, respectively, which encase the colon [100,101].

Primary Colorectal Cancer. Colorectal cancer (CRC) arises from multipotent stem cells found at the base of crypts following accumulation of genetic mutations and epigenetic changes [103–106]. Frequently mutated genes include adenomatous polyposis coli, Smad4, TP53, and PIK3CA [103]. Cancer lesions develop gradually: first, the mutated multipotent stem cells develop into premalignant polyps on the lining of the colon and rectum, then these polyps project into the lumen of the intestine, and eventually the tumor cells invade the mucosa (Fig. 6A, Table 1) [104,107]. CRCs can generally be categorized as microsatellite stable (MSS, ~85% of all CRC) or microsatellite instability-high (MSI-H, ~15% of all CRC). In MSI-H tumors, the DNA mismatch repair mechanism is dysfunctional, which leads to highly mutated, poorly differentiated tumor cells and a high infiltration of proinflammatory immune cells into the TME [103,105,106,108]. On the other hand, MSS tumors exhibit fewer mutations and have a TME that is largely absent of immune cells, but display more chromosomal abnormalities (deletions, amplifications, and translocations) and are more aggressive [103,105–107].

Tumor infiltrating immune cells play a key role in CRC tumor development and progression [109]. In fact, a metric known as the ImmunoScore—or, the density of immune cells in the tumor—predicts patient prognosis more accurately than traditional tumor staging [110,111]. In detailed recent studies, infiltration of the CRC TME by T helper 1 cells, M1 macrophages, dendritic cells, and NK cells has been linked to favorable patient prognoses, while the presence of M2 macrophages, MDSCs, T helper 17 cells, and B cells has been associated with poor outcomes [112–114]. The microbiome in the colon also influences inflammation and carcinogenesis in the tissue [115]. Imbalances and the presence of specific bacteria—for example, *Fusobacterium* [116]—support the development of CRC. The mechanisms behind these effects remain relatively unexplored, but may include secretion of metabolic byproducts, bacterial invasion of tissue, and interactions between bacteria and immune cells [115].

The positive feedback loop between CAFs and tumor cells is a distinguishing feature of the CRC TME. First, tumor cells secrete growth factors like platelet-derived growth factor, TNF, and FGF, which activate normal fibroblasts and promote differentiation towards CAF phenotypes; subsequently, CAFs become the main cellular component within the reactive tumor stroma [117,118]. Then, CAFs secrete chemokines like stromal cell-derived factor 1,

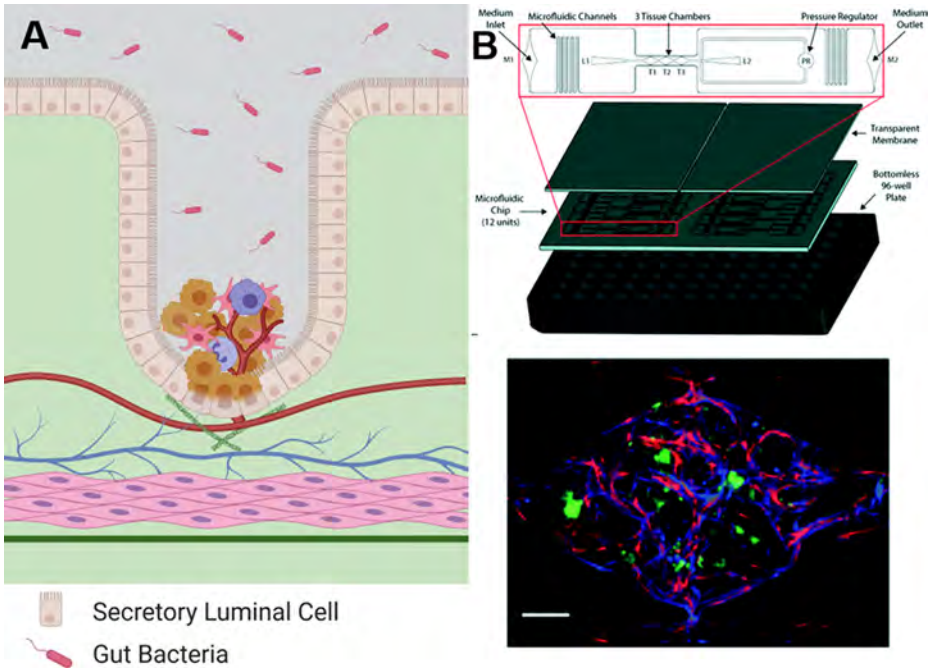

Fig. 6. Primary colorectal TME. (A) Colorectal cancers develop when the multipotent stem cells found at the base of crypts accumulate genetic mutations, chromosomal aberrations, and/or epigenetic changes. The CRC TME is characterized by a large CAF population and contact with the microbiome. (B) Our lab developed a high-throughput tumor-on-chip platform (top) [137]. Each tumor-on-chip model in the platform consisted of a vascularized TME (bottom), which included ECs (red), fibroblasts (blue), and CRC tumor cells (green). The device was used to study tumor cell crosstalk with stromal cells, gene expression, and response to therapy. J. Hachey, S. Movsesyan, Q.H. Nguyen, G. Burton-Sojo, A. Tankazyan, J. Wu, T. Hoang, D. Zhao, S. Wang, M.M. Hatch, E. Celaya, S. Gomez, G.T. Chen, R.T. Davis, K. Nee, N. Pervolarakis, D.A. Lawson, K. Kessenbrock, A.P. Lee, J. Lowengrub, M.L. Waterman, C.C.W. Hughes, An *in vitro* vascularized micro-tumor model of human colorectal cancer recapitulates *in vivo* responses to standard-of-care therapy, Lab Chip, 21 (2021) 1333–1351. - Published by The Royal Society of Chemistry. (For interpretation of the references to colour in this figure legend, the reader is referred to the web version of this article.)

hepatocyte growth factor, and VEGF; deposit collagen; and produce proteins that remodel the ECM. These conditions maintain CSCs, support tumor cell invasion and metastasis, and promote neovascularization [104,119–121]. Dysregulation of the TGFβ signaling pathway is a particularly prominent feature of the CAF-tumor cell feedback loop [104,117,120] and contributes to self-renewal of CRC CSCs [122], sustained tumor growth [122,123], induction of EMT [124,125], and resistance to chemotherapy [126].

Microfluidic Models of Colorectal Cancer. Recent microfluidic models mimic the physiology of the human colon. These models typically consist of adjacent channels separated by an ECM-coated membrane on which colon epithelial cells are grown [102]. Fluid flow through the cell-lined channel mimics movement of digested food and waste through the colon, and the models may also include cyclic mechanical stress simulating peristalsis [127], bacteria found in the microbiome [127–129], and/or geometry mimicking the crypt-villi architecture [130]. Like natural colon tissue, these models feature an absorptive epithelial barrier [127,128], support stem cell maintenance and differentiation [130], and produce mucus [127,129]. We also recently presented a model of a vascularized gut-on-chip that included perfused vessels, primary intestinal epithelial cells, and patient-derived gut myofibroblasts [131].

Additional microfluidic models of CRC have enabled examination of angiogenesis [75,76,132,133], nutrient gradients [134,135], stromal-tumor cell crosstalk [133,136,137], immunity [22,134,138–142], gene expression [137], response to therapy [75,76,132,136–141,143,144], and the microbiome [145] in the TME. For example, when CRC tumor cells in Matrigel were cultured in a circular chamber adjacent to colonic EC-lined channels, the ECs sprouted into the tumor chamber, mimicking angiogenesis in the TME. This model was also used to test nanoparticle-based delivery of the chemotherapy gemcitabine and analyze gene expression in tumor cells following therapy [132]. In a vascularized tumor-on-chip model wherein a self-assembled vascular network supports the growth of tumor cell lines (including those from CRC), we demonstrated that anti-angiogenic therapies inhibited tumor cell growth [76]. Ayuso and colleagues developed a microfluidic device with i) a large (millimeters wide) chamber filled with hydrogel-encapsulated cancer cells and ii) adjacent fluidic lines to mimic the blood vessels and deliver nutrients. They used the platform to demonstrate that hypoxia, limited nutrients, and low pH reduce proliferation and viability of the CRC cell line HCT-116 [134,135].

Microfluidic devices have also been used to reconstruct crosstalk between cell types in the CRC TME (Fig. 6B) [133,136–142]. Two independent studies cultured tumor cells and fibroblasts in adjacent channels of microfluidic devices and demonstrated that paracrine signaling [133] from and ECM deposition [136] by fibroblasts promotes growth and proliferation of CRC cell lines. In another microfluidic model of the CRC TME, Parlato and colleagues characterized the relationship between tumor cells and dendritic cells—which educate T cells through presentation of antigens following phagocytosis of tumor cells—in the absence and presence of novel anti-cancer therapy. The therapy increased dendritic cell migration towards and interaction with tumor cells, an effect regulated by the CXCR4/CCL12 signaling axis [138]. In a study from our group, we cultured a self-assembled vasculature in the central chamber of a device and patient-derived tumor cells in adjacent chambers. Co-culture of M1 macrophages in the tumor cell chambers reduced angiogenesis and tumor growth, while M2 macrophages facilitated angiogenesis, tumor growth, and tumor migration into the vasculature; these effects were mediated by soluble factors [142]. Additionally, patient- and murine-derived CRC spheroids cultured in perfused microfluidic devices retain their

tumor, stromal, and immune cell populations; mimic the *in vivo* response to checkpoint blockade immunotherapies; and can be used to screen novel therapies [139–141].

A handful of reports used microfluidic technology to couple the CRC TME to models of other organs, providing a systemic perspective on response to therapy [143,144] and metastasis [146,147]. Sung and colleagues cultured liver, CRC, and bone marrow cell lines in 3D hydrogels connected by fluidic lines. Following administration of the chemotherapy 5-fluorouracil, they characterized cell viability and drug concentration in each compartment and used the results to build a mathematical model describing the drug's pharmacokinetics and pharmacodynamics [143]. In related work, we cultured CRC cell spheroids and iPS-derived cardiomyocytes in microfluidic chambers separated by a channel lined with iPS-derived ECs to mimic the vasculature; we then evaluated the anti-cancer efficacy and cardiotoxicity of the chemotherapies doxorubicin and oxaliplatin. We found that both drugs reduced tumor growth and doxorubicin induced cardiotoxicity at its IC_{50}, while oxaliplatin required concentrations above its IC_{50} to do the same, matching clinical observations [144]. These models enable scientists and clinicians to quantify drug kinetics and dynamics and screen therapies for off-target effects in humanized and potentially personalized systems; further, they can be adapted to other tumor types and/or organ systems.

Future Directions. Most microfluidic models of CRC rely on cell lines; primary cell sources and more consideration of tumor category (i.e., MSI-H versus MSS) will improve the biological and clinical relevance of future models. Additionally, very few current models include CAFs, despite their prominence in the CRC TME. Future CRC models should also incorporate the colon-specific features—for example, flow through the colon, peristalsis, and the microbiome—found in microfluidic models of healthy colon tissue.

2.5. Pancreatic Cancer

Relevant Anatomy and Physiology. The pancreas is a long, slender organ located behind the stomach and between the duodenum—the first section of the small intestine—and the spleen. Structurally, the pancreas consists of a wide lobe next to the duodenum known as the "head"; the "body" of the organ tapers to a narrow "tail" located near the spleen. The pancreas tissue is composed of exocrine (>80% volume) and endocrine (<2% volume) tissues [148–150]. The exocrine tissue produces digestive enzymes which drain through the pancreatic duct into the duodenum, where they facilitate digestion and absorption of nutrients and neutralize stomach acid. The enzyme-secreting glandular cells are highly polarized, arranged into hollow acini, and capable of storing digestive enzymes for release following stimulation. The acini are connected through a series of ducts lined by cells that produce bicarbonate to neutralize stomach acid [149]. The endocrine tissue secretes hormones—namely, insulin, glucagon, and somatostatin—that regulate blood glucose levels. These cells are arranged into islets—also known as islets of Langerhans—which are interspersed throughout the organ and release their products directly into the blood stream [150,151]. The endocrine and exocrine structures are surrounded by pancreatic stellate cells, a specialized fibroblast that deposits ECM and supports each tissue's specialized structure [150]. The pancreas has a dual blood supply (celiac and superior mesenteric arteries) and is laced with sympathetic and parasympathetic nerves [149,150].

Primary Pancreatic Cancer. Pancreatic cancers originate in the exocrine cells (95% of cases) or endocrine cells (5% of cases) [152]. Pancreatic ductal adenocarcinoma (PDAC)—an adenocarcinoma of the exocrine cells lining the ducts, typically found in the head of the pancreas—is among the most aggressive, lethal, and difficult to treat cancers. Though PDAC is a rare disease, it is the third leading cause of cancer-related death in the United States because cases are often metastatic at diagnosis and largely refractory to current therapies [150,153–158]. Pancreatic neuroendocrine tumors develop in islet cells and offer more favorable patient prognoses [152].

The PDAC TME (Fig. 7A, Table 1) demonstrates a uniquely dense, fibrotic stroma [153,156,157,159,160]; hypovascularization [153,156,157,159]; hypoxia [153,160,161]; and immunosuppression [154,156,158,160]. ECM in the PDAC TME is dense, stiff, and rich in collagens, hyaluronic acid, and glycoproteins [153,156,159,160,162]. The abundance and composition of the ECM serve as a nutritional source for PDAC cells and promote tumor cell proliferation, migration, and invasion [159,160]. The density of the ECM, combined with water retention by glycoproteins, generates high interstitial fluid pressure in the pancreas, which prevents perfusion of the tumor and efficient delivery of

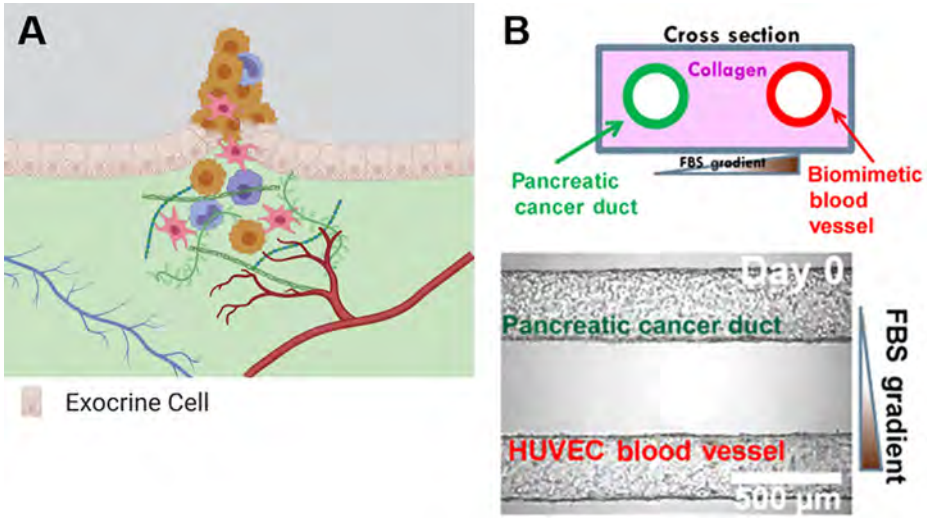

Fig. 7. Primary PDAC TME. (A) Pancreatic ductal adenocarcinomas form in exocrine cells that line the ducts and have a low mutational burden. The PDAC TME is characterized by its uniquely dense and abundant ECM; large populations of CAFs and immune cells; and hypovascularity accompanied by hypoxia. (B) To mimic the ducts and blood vessels present in the pancreas, Nguyen et al. [170] lined channels embedded in collagen gels with tumor cells (green) or ECs (red). The device was used to study tumor cell invasion into blood vessels. (For interpretation of the references to colour in this figure legend, the reader is referred to the web version of this article.)

anti-tumor therapeutics; hence, the ECM is a potential therapeutic target [155,159,160]. Hypoxia in the TME induces tumor cell EMT, invasion, and metabolic changes; activates CAFs; supports immunosuppressive TAMs and excludes proinflammatory T cells; and contributes to resistance to treatment [153,160,163–166].

The cellular component of the PDAC stroma is dominated by CAFs [159,162] but also includes immune cells, while tumor cells comprise a small minority of cells. Together, CAFs and immune cells can comprise > 50% of the tumor mass [156], a particularly unique feature of PDAC relative to other tumors. CAFs in the PDAC TME originate from pancreatic stellate cells and can take on multiple tumor phenotypes [153,162]. Inflammatory CAFs deposit the ECM and promote tumor growth and neoangiogenesis. Myofibroblast CAFs establish immunosuppression in the TME; for example, they secrete granulocyte–macrophage colony-stimulating factor to recruit macrophages [162]. The immune infiltrate in the PDAC TME is predominantly immunosuppressive MDSCs, TAMs, and Tregs [156,158,160,165]. The MDSCs are recruited to the tumor from the bone marrow when PDAC tumor cells co-opt chemokine pathways like CCL2/CCR2 and CXCL1-3/CXCR2 [167,168]. PDAC tumor cells have a low mutational burden and the TME is largely devoid of T cells; however, some tumors display high T cell infiltration and these patients have better clinical outcomes [154,158,165,169].

Microfluidic Models of Pancreatic Cancer. Recent work has capitalized on microfluidic technology to mimic the PDAC TME's distinctive physiochemical properties [170–172], cell–cell interactions [170,171,173–176], and resistance to therapy [171–173,175,176]. For example, Nguyen and colleagues introduced a collagen hydrogel-filled device that includes adjacent channels, one filled with PDAC cells in a hydrogel and the other lined with EC cells (Fig. 7B). The team used the device to probe the paradox presented by PDAC's early metastasis and apparent hypovascularity, and found that PDAC cells migrate towards and invade into the vascular channel, where they kill ECs and eventually fill the channel. Further, the team demonstrated that activin-ALK7 signaling mediates this process and replicated their findings in mice [170]. Kramer et al. [172] developed a high-throughput microfluidic device with controllable and quantifiable interstitial flow. In this device, PDAC cells cultured under high interstitial pressure were viable but less proliferative than cells cultured under normal perfusion conditions. Further, tumor cells under high interstitial pressure were resistant to the common treatment gemcitabine, which the research team attributed to upregulation of MRP efflux transporters rather than exclusion of the drug from the TME. This model provides unique insight on the role of high interstitial pressure in the PDAC TME. Lee and colleagues cultured pancreatic stellate cells and PDAC spheroids in adjacent chambers of a collagen hydrogel-filled microfluidic device. The pancreatic stellate cells enhanced tumor cell growth, EMT, and migration and modified the response to common chemotherapies; meanwhile, PDAC cells differentiated PSCs to an activated phenotype that included increased growth and migration and a spindle-like morphology [171]. Additional studies have shown that PDAC cell lines cultured in microfluidic platforms mimic *in vivo* PDAC TME cell–cell interactions [173–176], EMT [174,177], ECM remodeling [174,176], and response to chemotherapies [173,175–177].

Future Directions. The current generation of microfluidic devices used to model the PDAC TME lack several distinct features of the tumor, including the immune cell infiltrate, hypoxia, and the dynamic and overwhelming desmoplastic stroma. These models also typically use cell lines—some of which are derived from mice—and future iterations should prioritize the use of human and primary cell sources. Further, a PDAC TME model integrated with a bone marrow tissue model would permit studies of the recruitment of myeloid cells from the bone marrow to the tumor, which is believed to be a primary mechanism for development of immunosuppression in the PDAC TME.

2.6. Skin Cancer

Relevant Anatomy and Physiology. The primary role of the skin is to provide a barrier between the environment and the organism; it acts as a physical barrier and provides a unique immune system responsive to trauma, pathogens, and external stimuli/stressors (for example, ultraviolet (UV) light). The organ also regulates temperature and hydration, transmits sensation, and stores nutrients [178–180]. The skin is a few millimeters thick and has three layers: the epidermis, dermis, and hypodermis [178]. The epidermis, which directly interfaces with the environment, is an avascular sheet composed of keratinocytes, basal cells, melanocytes, and immune cells [178]. The inner layer of the epidermis is dominated by rapidly reproducing, rounded basal cells. As these cells travel towards the surface of the epidermis, they mature into stratified keratinocytes—also known as squamous cells—that produce keratin, a hard protein that protects the organism from physical threats. Humans constantly shed dead keratinocytes from the surface of the skin [178,180]. Melanocytes produce the pigment melanin, which protects the organism from UV light [178]. The dermis is a dense layer that hosts blood and lymphatic vessels, nerves, fibroblasts, and immune cells [178,179]. The hypodermis is a vascularized layer of fat tissue separating the skin from the musculoskeletal system [178,180]. The skin has an abundant ECM—composed of collagen, proteoglycans, and elastin—which gives the organ its distinctive flexibility [178–180]. The organ is also interspersed with cells and structures related to the autonomic nervous and auto/paracrine systems (e.g. hair follicles and sebaceous glands) [178].

Primary Skin Cancer. Skin cancer is the most commonly diagnosed cancer, and the large majority of these lesions arise from squamous cells, basal cells, or melanocytes [181,182]. These cancers can be found in any cutaneous location, but are most common in sun exposed areas (i.e., back, face, and shoulders). UV radiation from the sun plays a key role in skin carcinogenesis; specifically, UV radiation penetrates the skin and damages cells and DNA [182]. Basal and squamous cell skin cancers account for ~ 75% and ~ 20% of cases, respectively, and are very treatable. Though melanomas—which originate in melanocytes—account for only 1% of diagnosed skin cancers, they are more aggressive and thus are a primary focus of current skin cancer research. Less common skin cancers include Merkel cell carcinoma, skin lymphoma, and Kaposi sarcoma [181].

Basal and squamous cell carcinoma cells frequently carry UV-induced mutations in oncogenes like TP53 and Ras [183]. In fact, genomic instability—from UV-induced mutations and double-stranded DNA breaks, human papillomavirus virus, and telomerase aberrations—appears to be the driving force behind carcinogenesis in basal and squamous cell carcinoma cells [182,183]. Since these tumors are typically easy to remove and less aggressive, there is little information available about other features of the TME.

Melanoma (Fig. 8A, Table 1) typically arises from a congenital nevus (mole), in a benign-to-malignant tumorigenesis process that includes gaining the ability to proliferate, invade the surrounding tissue, and metastasize to distant organs [184]. Like basal and squamous cell carcinomas, melanomas often develop following UV light exposure and exhibit a high tumor mutational burden [181,182]. Specifically, many melanomas exhibit a BRAF mutation, which often results in downstream mitogen-activated protein kinase activation and tumor growth [181,184]. Melanoma cells downregulate expression of E-cadherin—which normally mediates interactions between melanocytes and keratinocytes—and upregulate expression of N-cadherin—which enables interactions with

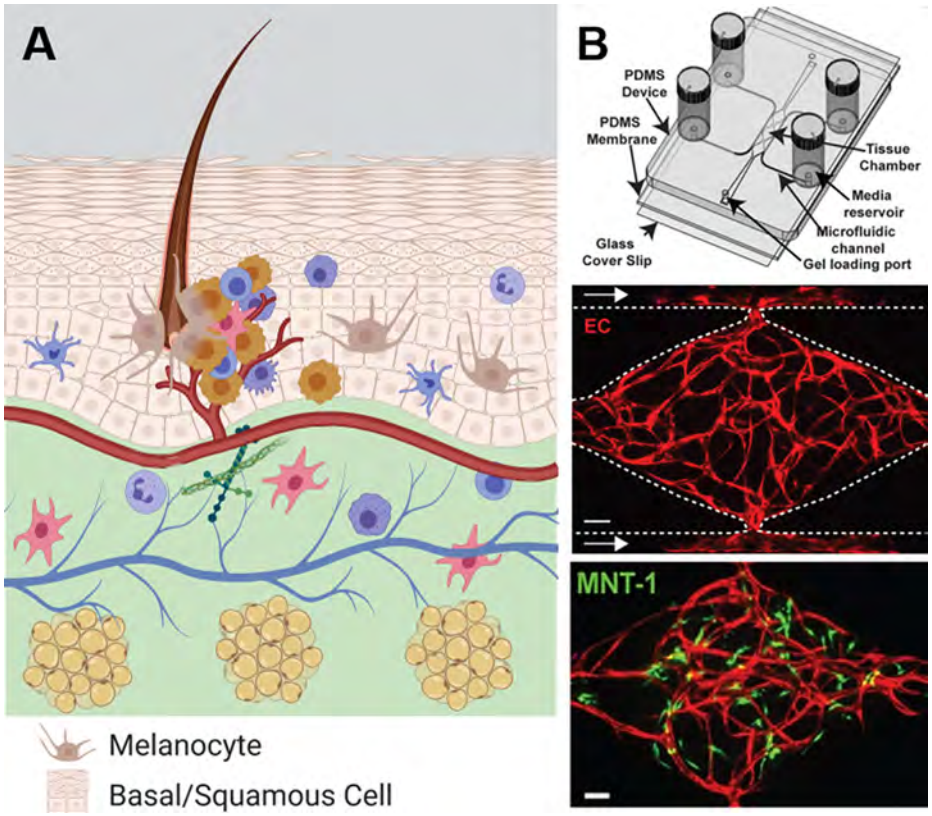

Fig. 8. Primary melanoma TME. (A) Melanoma skin cancers stem from UV-damaged, highly mutated melanocytes found near hair follicles (shown here) or in moles. The melanoma TME is characterized by an abundant immune cell infiltrate that includes TAMs, neutrophils, NK cells, dendritic cells, and cytotoxic T cells; a remodeled ECM rich in collagen, fibronectin, and laminin; and angiogenesis. (B) ECs and stromal cells suspended in a hydrogel and exposed to interstitial flow self-assembled into perfused vascular networks (red). The melanoma cell line MNT-1 was added to the system to model the vascularized TME [76]. (For interpretation of the references to colour in this figure legend, the reader is referred to the web version of this article.)

ECs and fibroblasts. Together, these changes in cadherin expression facilitate tumor cell proliferation, motility, invasion, and metastasis [184]. Melanoma cells promote conversion of fibroblasts to CAFs through secretion of platelet-derived growth factor, FGF2, and TGFβ. Subsequently, CAFs deposit collagen, fibronectin, and laminin ECM proteins; promote angiogenesis; and secrete growth factors like FGF2 and insulin-like growth factor 1 that support continued tumor cell growth and proliferation [184]. CAFs can also establish CXCL9, CXCL10, and CXCL11 chemokine gradients to recruit effector T cells or secrete MMPs and prostaglandin E2 to suppress cytotoxic NK cell activity [185]. Melanoma's high tumor mutational burden renders the TME highly immunogenic: initial disease progression is marked by infiltration of anti-tumor TAMs, neutrophils, NK cells, dendritic cells, and cytotoxic T cells into the tumor. To evade this strong immune response, tumor cells evolve to reduce expression of major histocompatibility complex proteins and neoantigens; suppress the activity of anti-tumor neutrophils and T cells; and promote differentiation of resident TAMs and neutrophils to pro-tumor phenotypes [185]. Notably, checkpoint blockade therapies like PD-1 and CTLA-4 inhibitors and cytokine stimulation with IL-2 or interferon α can reinvigorate the anti-tumor immune response in 30–60% of melanoma patients [185–190]. In fact, the success of checkpoint blockade therapies in melanoma patients heralded the current immunotherapy revolution and was recognized with the 2018 Nobel Prize in Physiology or Medicine [185,191].

Microfluidic Models of Skin Cancer. Multiple microfluidic models recreate the normal anatomy and physiology of the skin (reviewed in [179,180]). First generation microfluidic models extended the lifetime of commercially available skin constructs—typically composed of primary dermal and/or epidermal cells embedded in ECM-mimetic hydrogels [192]—through the addition of perfusion [179,192–194]. More recent models pattern keratinocytes, fibroblasts, and/or ECs to mimic native organ architecture [180,195,196] and may incorporate hair follicles, adipocytes, mechanical strain, or fluidic connections to other organs [179,180]. These platforms have primarily been used to study skin biology, drug transport and response, and inflammation [179,180].

Despite a plethora of microfluidic devices modeling the skin, only a few platforms have been adapted to the study of skin cancer. In a 2021 report, keratinocytes, melanoma cells, and fibroblasts were cultured in adjacent chambers of a microfluidic device. Cross-talk between tumor cells and normal cells in the device altered tumor cell morphology and metabolism; additionally, keratinocytes and fibroblasts secreted chemokines—including IL-6, IL-8, IL-1β, and IL-1α—that support tumor cell growth [197]. Businaro et al. [198] cultured melanoma cells and murine spleen cells at opposite ends of a fluid-filled channel. They showed that expression of the transcription factor interferon regulatory factor 8 in spleen cells promotes spleen cell migration towards and interaction with melanoma cells and inhibits tumor cell migration and invasion. Another report cultured melanoma cells resistant and sensitive to the drug vemurafenib—which targets mutant BRAF—on either side of a 100 μm-wide poly(ethylene glycol) hydrogel barrier. The results demonstrated that vemurafenib-resistant melanoma cells can confer resistance on previously sensitive cells via paracrine FGF2 signaling [199]. Additional studies have cultured melanoma cell lines in microfluidic devices to study tumor growth (Fig. 8B) [76,133] and response to therapy [97,200].

Future Directions. Current microfluidic models of skin cancer are simplistic relative to those of healthy skin. Future iterations should seek to mimic native tissue architecture; incorporate multiple cell

types, the vasculature, and lymphatics; and include mechanical strain and an air-tissue interface. Additionally, current models are restricted to melanoma cell lines. Studies that utilize primary cell sources and consider nonmelanoma cancers may provide additional insight on carcinogenesis and metastasis in the skin. Further, characterization of immune-tumor cell interactions in melanoma—the prototypical candidate for immunotherapy—with the high spatiotemporal resolution offered by microfluidic models may help explain the variable response rates in this and other cancers.

3. Metastatic Sites

3.1. Liver

Relevant Anatomy and Physiology. The liver is the largest organ in the body and consists of two lobes covered by the Glisson capsule—the visceral peritoneum of the liver [201,202]. It has multiple functions, including carbohydrate transformation and storage; detoxification of endogenous and exogenous substances; and synthesis of cholesterol, bile salts, immune complement components, and cytokines/chemokines [8,202–204]. The liver has a dual blood supply: the portal vein system carries deoxygenated blood rich in nutrients and toxins and constitutes 75–80% of the organ's blood supply; while the hepatic arteries deliver oxygenated blood and account for the balance of the supply [8,201,202,205]. Parenchymal cells—namely, hepatocytes and cholangiocytes—constitute 70% of the cells in the organ and are responsible for the metabolic, detoxification, and synthesis processes that take place in the liver [8,205]. The hepatocytes are organized into plates which are interlaced with sinusoids, the liver's specialized vasculature [202]. Sinusoids are tortuous and highly permeable vessels that lack a basement membrane and are lined with fenestrated liver sinusoidal endothelial cells (LSECs). The permeability of the sinusoids facilitates the necessary exchange of nutrients and waste between the blood and the liver parenchyma [8,202,204]. The sinusoidal lumen contains Kupffer cells—a liver-specific macrophage that constitutes ~ 10% of the organ's cells—and NK cells, which together represent the organ's first line of immune protection [203,204,206]. Other immune cells in the organ include T cells, dendritic cells, mast cells, and neutrophils [203,204]. The space between the hepatocyte plates and sinusoids, known as the perisinusoidal space or space of Disse, contains hepatic stellate cells. Hepatic stellate cells are typically quiescent and store vitamin A and nutrients; they become activated following damage to the liver and orchestrate the subsequent self-renewal process [202,205]. Notably, the liver has the capacity to replace up to 70% of its original volume [202].

Metastasis to the Liver. The liver is the most common site of metastasis, and liver metastases are far more common than primary liver tumors. Primary tumors that frequently metastasize to the liver include cancers of the gastrointestinal tract (i.e., CRC and pancreatic cancer), BC, lung cancer, and melanoma [8,206,207]. Multiple characteristics of the liver enable the development of metastatic lesions (Fig. 9A, Table 2): i) the organ has a dual blood supply, is highly vascularized, and experiences a large total volume of blood flow; and ii) the sinusoids feature fenestrated LSECs, are highly permeable, and experience slow rates of blood flow [8,202].

Exosomes secreted by the primary tumor further condition the liver for metastasis by increasing vessel permeability, activating local fibroblasts, and recruiting bone marrow-derived immune cells to the niche [8,206]. For example, when Kupffer cells absorb exosomes containing macrophage migration inhibitory factor, they express TGFβ; the soluble factor activates hepatic stellate cells in the space of Disse, which subsequently recruit tumor-promoting macrophages from the bone marrow [8,206,207]. Activated hepatic stellate cells also initiate fibrotic processes involved in liver repair, including production of collagen I & IV-rich ECM and angiogenesis [8,206]. The stiffer ECM promotes tumor cell survival and growth [207].

CTCs arriving in the liver initially encounter Kupffer and NK cells in the lumen of the sinusoids. Both of these cells display potent cytotoxicity towards tumor cells and represent a challenging obstacle to metastasis. However, CTCs occasionally evade these immune cells, bind to LSEC adhesion receptors (i.e., E-selectin, vascular cell adhesion molecule 1, and intercellular adhesion molecule 1), and extravasate into the space of Disse [8,206]. When CTCs

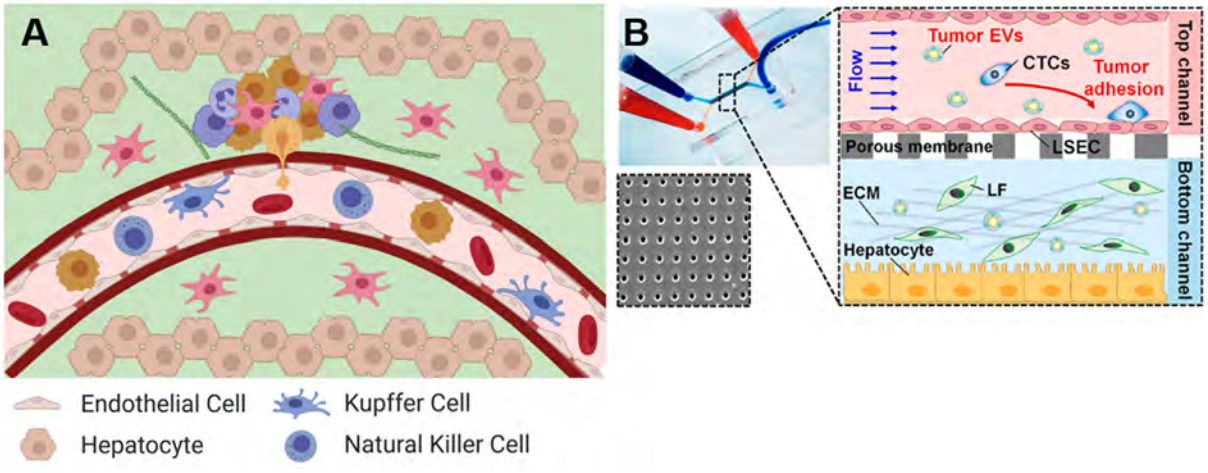

Fig. 9. Metastatic liver TME. (A) CTCs in the liver encounter Kupffer and NK cells in the sinusoids and extravasate through a fenestrated, highly permeable endothelial barrier into the space of Disse. Metastatic lesions grow between the sinusoids and hepatocyte plates and are supported by activated hepatic stellate cells (i.e., CAFs). (B) To study BC metastasis to the liver, Kim and colleagues developed a two-chamber microfluidic model of the liver [208]. The lower chamber, which mimics the space of Disse, was filled with hepatic stellate cells embedded in hydrogel and lined with hepatocytes on the bottom wall. The upper chamber was lined with LSECs and perfused with fluid to model the sinusoids. Reprinted (adapted) with permission from J. Kim, C. Lee, I. Kim, J. Ro, J. Kim, Y. Min, J. Park, V. Sunkara, Y.S. Park, I. Michael, Y.A. Kim, H.J. Lee, Y.K. Cho, Three-Dimensional Human Liver-Chip Emulating Premetastatic Niche Formation by Breast Cancer-Derived Extracellular Vesicles, ACS Nano, 14 (2020) 14971–14988. Copyright 2020 American Chemical Society.

Table 2
A summary of the organ-specific features of common metastatic sites.

Metastatic Site	Prominent Features
Liver	• Highly vascularized with dual blood supply • Very permeable sinusoid vessels with fenestrated ECs • Large population of macrophages • Remodeled ECM rich in collagen I & IV • Hypoxia
Lung	• Highly vascularized with dual blood supply • Abundance of immunosuppressive cells, including macrophages and neutrophils • Angiogenesis
Bone	• Highly vascularized • Very permeable blood vessels • Large populations of fibroblasts and immature immune cells • ECM composed of collagen I and rich in minerals, growth factors, and cell adhesion molecules • Hypoxia
Brain	• Highly vascularized • Blood-brain barrier restricts entry of cells and soluble factors • Small population of immune cells, primarily astrocytes and microglial cells • Hypoxia, limited nutrients

begin to establish themselves in the liver, Kupffer cells switch from inhibiting to promoting metastasis. Instead of phagocytosing tumor cells, Kupffer cells upregulate adhesion receptor expression in LSECs, produce chemokines that promote tumor cell proliferation and invasion, and can facilitate angiogenesis [8,206,207]. In the space of Disse, metastasizing tumor cells establish lesions that become infiltrated with bone marrow-derived neutrophils, Tregs, and MDSCs. Tumor cells can bind to hepatocytes and their ECM [206], but the precise role of hepatocytes in the metastatic cascade is currently under characterized [8]. As the metastatic lesion grows, it displaces and kills hepatocytes and requires additional nutrient support (acquired through cooption of existing blood vessels or, less frequently, angiogenesis) [8].

Microfluidic Models of Liver Metastases. Multiple microfluidic platforms model metastasis to the liver [146,147,205,208–213]. Kim and colleagues recreated liver sinusoid architecture in a two-channel device (Fig. 9B). Bounded by hepatocytes lining the bottom and a porous membrane at the top, the lower chamber is filled with liver fibroblasts embedded in Matrigel. The team showed that introduction of extracellular vesicles from BC cell lines into the upper chamber alters LSEC phenotype—namely, expression of tight junctions decreases while that of mesenchymal markers increases. These changes emulate primary tumor conditioning of the metastatic niche as shown by the fact that BC cells introduced into the upper chamber bind to these altered LSECs at higher rates. Further, the team shows that BC cell binding to LSECs depends on physiochemical features of the liver microenvironment, the identity of the primary tumor, and the extracellular vesicle cargo protein TGFβ1 [208]. In a 2016 report, two hydrogel compartments modeling CRC and liver tissues were connected by a micro-peristaltic pump. The platform was used to study metastatic spread of CRC cells to the liver and to screen potential anti-cancer drugs [147].

The commercially available "LiverChip" system consists of primary parenchymal and non-parenchymal hepatic cells cultured at physiologically-relevant ratios in a 3D, perfused microfluidic chamber [205,209–211]. In addition to recreating the normal physiological functions of the liver [205,209,210], this system has been extensively employed to study metastatic seeding in the organ. Following introduction of BC cell lines to the tissue chamber, the platform mimics dormancy of tumor cells in the liver [209] and demonstrates the influential role of scaffold stiffness on dormancy, inflammation, and tumor cell response to chemotherapy [211]. Further, treatment of the LiverChip with BC-derived exosomes enables more tumor cells to establish themselves in the niche; however, hepatic cell-derived exosomes counter this effect by reducing tumor cell growth, proliferation, and invasiveness [211].

Future Directions. A model of the liver metastatic niche should include the liver microarchitecture (sinusoids, space of Disse, and plates of hepatocytes), the liver-specific population of immune cells, and a microfluidic connection to the primary TME. Currently available models typically include only one of these features and largely ignore immune cell populations—including Kupffer cells, which are known to play a key role in metastasis to the liver. Further, most of these models use cell lines and study BC; future work should seek to incorporate primary cells and a variety of primary cancers, which may inform future therapeutic strategies.

3.2. Lung

Metastasis to the Lung. Section 2.1 summarized the basic anatomy of the lung, including a seminal feature that plays a major role in the lung as a site for metastatic cancer: the entire cardiac output from the right side of the heart passes through the pulmonary circulation. This anatomical feature renders the lung as a site of metastasis through two mechanisms. First, CTCs in the venous circulation or the lymphatic circulation (which empties into the venous circulation prior to entering the right atrium) are delivered directly to the microcirculation of the lung, where they can potentially become trapped or lodged. Second, primary tumor-derived soluble factors or extracellular vesicles produced in any other organ are emptied into the venous circulation; thus, the lung is the first site where these tumor-derived products can impact the local microenvironment to create a favorable site for metastasis. This latter process has been dubbed the pre-metastatic niche [12,214,215]. The pre-metastatic niche in the lungs is generally thought to be initiated by soluble factors or extracellular vesicles derived from the primary tumor that encourage the recruitment of bone marrow-derived leukocytes (e.g., macrophages and neutrophils) to the lung and remodeling of the ECM [12,216–219]. The presence of these immune cells in the lung creates a favorable environment for tumor cell seeding and growth by stimulating angiogenesis and creating an immunosuppressive microenvironment. As a result, the lungs are the second most common site for metastatic tumors (Fig. 10A, Table 2) accounting for roughly 20–50% of all cases [220]. The most common primary tumors to metastasize to the lung are BC, CRC, renal cancer, and head and neck cancer.

Microfluidic Models of Lung Metastases. Modeling metastasis of tumors to the lungs has relied heavily on the use of mouse models, in particular tail vein injection of CTCs, which travel directly to the lungs. While numerous microfluidic models have attempted to simulate essential features of metastasis including extravasation [221–229], only a few reports attempt to specifically model the metastasis of tumors to the lungs using microfluidic models. A 2019 model created a multi-organ chip to simulate lung metastasis by linking a primary CRC chamber to chambers representing the liver, lungs, endothelium, and a hydrogel control; all tissues were modeled using common cell lines (Fig. 10B). The CRC cells preferentially migrated to the lung and liver chambers, mimicking the metastatic patterns observed in CRC patients [146]. In a 2016 model, a porous membrane separated primary lung or muscle cells from a human umbilical vein EC-lined channel which was perfused with CTCs from BC and salivary gland cancers. The CTCs preferentially bound to the endothelium adjacent to primary lung versus

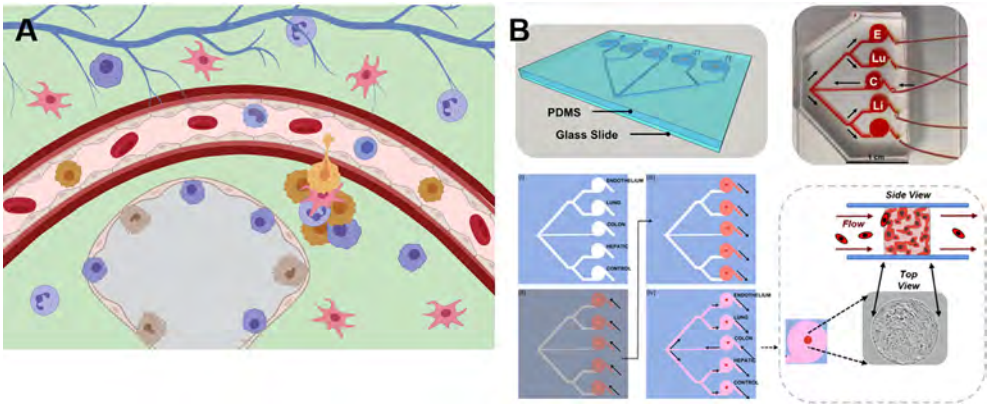

Fig. 10. Metastatic lung TME. (A) CTCs in the lung extravasate into the tissue adjacent to alveoli. Tumor-derived soluble factors and exosomes pre-condition the tissue for metastasis. The metastatic lesion is infiltrated by immunosuppressive cells—i.e., macrophages and neutrophils—which permit and support tumor cell growth. (B) To study metastasis of CRC cells, lung epithelial cells (Lu), hepatic cells (Li), ECs (E), and CRC cells (C) embedded in hyaluronic acid/gelatin hydrogels and an empty hydrogel control (not labeled) were cultured in fluidically linked chambers [146].

muscle cells, and treatment with the small molecule metastasis inhibitor AMD3100 dramatically reduced cell attachment. In subsequent experiments, the lung cells were replaced with primary bone or liver cells [212].

Future Directions. There has been very limited progress in modeling metastasis to the lungs; thus, there are many opportunities to advance the field. Models should attempt to include the most salient anatomical features of the lung, including lung-specific ECs, stromal cells, and macrophages; cyclic mechanical strain; and the air-tissue interface. Finally, future models should incorporate primary cell sources and compare and contrast the major cancers that metastasize to the lungs.

3.3. Bone

Relevant Anatomy and Physiology. The bone marrow is the primary site of hematopoiesis and also plays a central role in bone remodeling [230]. Hematopoiesis, or the production of all blood cell types, occurs through maturation and differentiation of hematopoietic stem cells (HSCs). HSCs are maintained in quiescent and self-renewing states in the bone marrow and can differentiate into erythroid, lymphoid, and myeloid lineage blood cells [231,232]. Bone remodeling is a continuous process that occurs at the surface of bones and requires a precise balance between the activity of osteoblasts—or, bone forming cells—and osteoclasts—or, cells that resorb bone [233,234].

Bone marrow tissue resides at the core of bones [234] and is characterized by a heterogenous, dense cellularity [230]. Cells of the bone marrow include HSCs, immature and mature blood cells, ECs, and mesenchymal stem/stromal cells (MSCs) [230,234]. ECs in the bone marrow form dense vascular networks [230,235]. MSCs are self-renewing progenitor cells that give rise to many non-hematopoietic cells found in the bone marrow, including osteoblasts, adipocytes, and chondrocytes [230,234]. The extracellular matrix in the bone marrow is composed of 90–95% Type I collagen supplemented by calcium salt deposits, the mineral hydroxyapatite, growth factors, and proteins involved in cell adhesion [7,233,234]. The bone marrow microenvironment is hypoxic relative to other tissues in the body [230].

Metastasis to the Bone. Multiple features of the microenvironment promote metastasis to the bone marrow (Fig. 11A, Table 2)

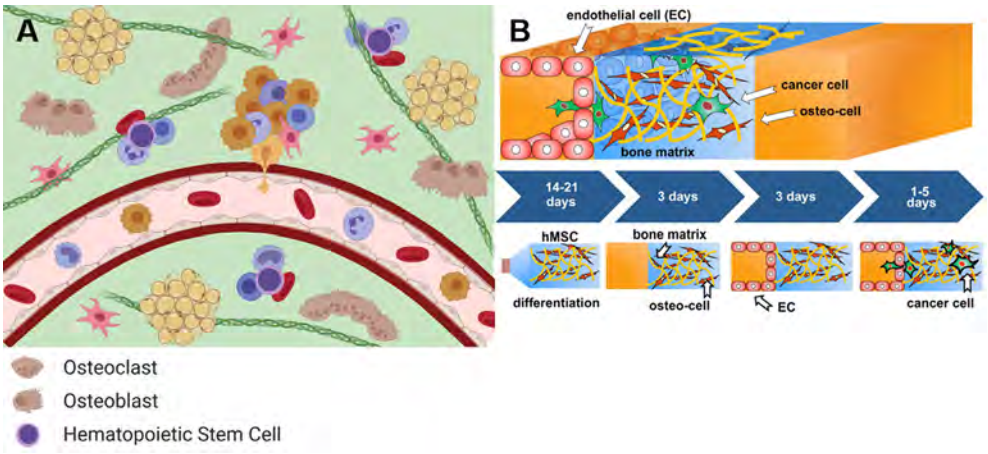

Fig. 11. Metastatic bone TME. (A) CTCs in the bone marrow extravasate through the highly permeable endothelial barrier into a densely cellular space populated with HSCs, immature immune cells, fibroblasts, and adipocytes. The environment is hypoxic and rich in collagen I, minerals, growth factors, and cell adhesion molecules. Metastatic lesions are supported by dysregulated osteoblasts or osteoclasts. (B) This 2014 bone marrow microfluidic model consisted of two adjacent chambers [222]. The chamber at right (blue) was filled with MSCs embedded in a hydrogel to mimic the bone marrow tissue. The chamber at left (yellow) was lined with ECs and perfused with media to replicate a blood vessel. BC cells perfused through the blood vessel chamber can metastasize into the tissue chamber. (For interpretation of the references to colour in this figure legend, the reader is referred to the web version of this article.)

[7,230,233,234]. Due to its characteristic dense vascular network, the bone marrow experiences high blood flow, increasing the opportunity for CTCs to extravasate from a blood vessel into the tissue [233]. This vascular network is also quite permeable [235], which further facilitates tumor cell extravasation. After a CTC exits the vasculature, it encounters a microenvironment rich in adhesive molecules and immobilized growth factors; these conditions favor tumor cell attachment, survival, and proliferation [7,233,234].

Many solid tumors metastasize to the bone marrow and these metastases disrupt the normal bone remodeling process [7,233,234]. In osteolytic metastases, tumor cells activate osteoclasts, which break down the bone matrix and release growth factors, thereby generating a niche conducive to tumor cell survival and growth [7,233]. Conversely, osteoblastic metastases are characterized by overactivation of osteoblasts and subsequent formation of bone matrix; however, the mechanisms governing this process remain poorly understood [233,234]. Approximately 70% of BC and PCa patients experience metastasis to the bone [7,233,234]; the majority of BC patients experience osteolytic metastases, while PCa patients experience predominantly osteoblastic lesions.

Microfluidic Models of Bone Metastases. In the last decade, a number of studies have utilized microfluidic devices to recreate the physiology of the bone marrow microenvironment. These platforms typically include primary bone marrow MSCs embedded in a bone-mimetic matrix cultured under perfused media conditions; this construct can be supplemented with vascular networks and/or HSCs. Popular bone-mimetic matrix choices include decellularized bone scaffolds [236], collagen I [222,237,238] (which may be supplemented with proteins like bone morphogenetic protein 2 and 4 [239,240]), hydroxyapatite-coated zirconium oxide ceramic [241], hydroxyapatite-gelatin [242], and fibrin [224,243,244]. To recreate the native bone marrow vasculature, researchers use one of two approaches: either i) the channel of a microfluidic device is seeded with ECs and perfused with media (Fig. 11B) [222]; or ii) ECs and MSCs are cultured in a hydrogel or matrix to promote self-assembly of vascular networks [224,244]. HSCs are sourced from either primary bone marrow [239,240,242,243] or primary cord blood samples [241,244]. Notably, these microfluidic models of the bone marrow microenvironment can maintain HSCs and support hematopoiesis [239–243], a feat that is not possible in traditional *in vitro* systems. These microfluidic models also enable observation of cellular events in the bone marrow with a spatiotemporal resolution that is impossible in mouse models.

These microfluidic models of the healthy bone marrow microenvironment have also been adapted to the study of pathological processes, including primary cancer [237,242,245], cancer metastasis [212,213,222,224,236,238,244,246], and response to pharmaceuticals and radiation [236,239,240,243,246]. For example, a pair of papers from the Kamm lab perfused BC cells through EC-lined microfluidic channels (Fig. 11B) [222] or self-assembled vasculature cultured in microfluidic devices [224]. They observed that more cells extravasate across the endothelium and that these cells migrate further into adjacent tissue chambers when the tissue includes human bone marrow-derived MSCs (control tissues included muscle-mimetic self-assembled vasculature and empty hydrogels). These studies also replicated the role of the CXCL5-CXCR2 signaling axis in enabling BC extravasation to the bone marrow [222] and adenosine A3 receptor in preventing BC metastasis to the muscle [224]. Marturano-Kruik and colleagues seeded ECs and MSCs into decellularized 3D bone matrices and cultured them in perfused microfluidic devices to recreate the bone marrow microenvironment [236]. BC cells introduced into this system demonstrated a decreased cancer cell growth rate—that is, dormancy—and an increased resistance to the commonly used chemotherapy sunitinib; both of these observations are consistent with the behavior of BC cells at metastatic bone marrow sites *in vivo*. Further, metastatic BC cells demonstrated enhanced extravasation [224] and tissue remodeling [238] relative to non-metastatic BC cells in bone marrow microfluidic models.

Future Directions. Hypoxia is a distinguishing feature of the bone marrow microenvironment and is known to modulate cell phenotype, but most current microfluidic models are cultured at ambient oxygen levels. Additionally, the current bone marrow metastasis models rely on cancer cell lines and focus on BC, while the behavior of primary CTCs and cells from other solid tumors known to metastasize to the bone (i.e., PCa) remain uncharacterized. Finally, metastasis is an unusual event involving, at most, a handful of cells extravasating into a tissue and establishing a colony. Current metastasis models overwhelm the tissue model with cancer cells, which may obscure detailed features of metastasis under the physiological dilute ratio of tumor cells to bone marrow.

3.4. Brain

Relevant Anatomy and Physiology. The brain is the control center of the nervous system and its primary function is to protect and support neurons, the cells responsible for transmitting signals through the brain and to the spinal cord and the rest of the body [15,247]. Neurons demand a relatively high amount of oxygen and glucose, resulting in a partial pressure of only 35 mmHg (~4.6% oxygen) and limited nutrients in the brain parenchyma. Proper functioning of the brain relies on the maintenance of a stable microenvironment around neurons by the blood–brain barrier (BBB), a vascular network that surrounds neurons and strictly limits the free movement of molecules and cells between the blood and the brain tissue. Four components work together to generate this barrier, which together is termed the neurovascular unit: specialized ECs are connected by extensive tight junctions and display low pinocytotic activity with high expression of efflux pumps; dense pericytes surround the capillaries; a double-layered basement membrane encapsulates the ECs and pericytes; and astrocytes wrap foot processes around the entire vessel structure [15,247–249]. Astrocytes regulate homeostasis in the brain parenchyma through transport of solutes, and transport and metabolism of glutamate and γ-aminobutyrate [247,249]. While small lipophilic molecules such as oxygen and caffeine can cross the BBB with relative ease, most molecules have to be actively transported across the endothelium; hence, brain ECs express numerous transporters for necessary nutrients, including glucose and amino acids [250]. The brain is further protected by microglial cells, or brain-specific macrophages that regulate immunity in the brain through secretion of chemokines and phagocytosis [15,247]. Finally, the organ is bathed in the cerebrospinal fluid, which allows for exchange of nutrient and waste molecules between the body and brain and is usually immunosuppressive [247,249].

Metastasis to the Brain. The metastatic spread of cancer to the brain is a devastating diagnosis, with an average survival time of less than a year. Somewhere between 10 and 30% of newly-diagnosed cancers will ultimately metastasize to brain, with the most common being lung cancer, melanoma, BC, renal cancer, and CRC [9,15,247,251]. The vast majority (>95%) of brain metastases are found in the brain parenchyma, though a minority—known as leptomeningeal metastases—are located in the blood-cerebrospinal fluid or the protective membrane that surrounds the organ [15].

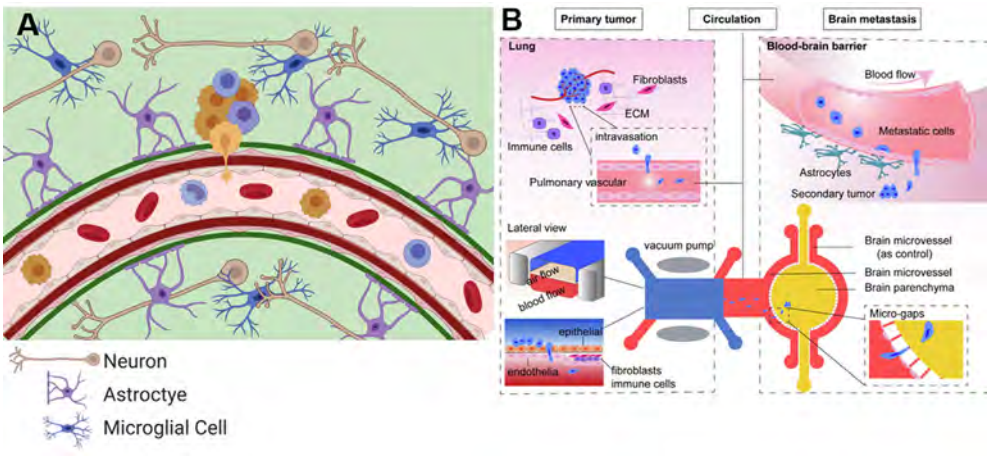

Fig. 12. Metastatic brain TME. (A) CTCs in the brain encounter the blood–brain barrier—a unit of organ-specific ECs surrounded by pericytes, a basement membrane, and astrocytes that restricts movement of cells and molecules into the organ parenchyma. Cells that overcome this barrier to extravasation encounter a hypoxic, nutrient-poor environment populated by neurons, microglial cells, and astrocytes. Metastatic lesions adopt an altered metabolism and coopt the vasculature and astrocytes to support tumor cell survival and growth. (B) Microfluidic models of the lung and brain were fluidically linked to study NSCLC metastasis [260]. The lung model included an air-tissue interface consisting of epithelial and endothelial cells cultured on opposite sides of a permeable membrane, cyclic mechanical strain, and NSCLC cells. In the brain model, astrocytes embedded in hydrogel were cultured in a circular chamber surrounded by channels lined with brain-specific ECs. Metastasizing NSCLC cells traveled from the lung compartment to that of the brain through the fluidic lines.

Much like other common sites of metastasis, the brain is densely vascularized and experiences relatively high blood flow [15]. However, the BBB's considerable barrier to entry and the brain parenchyma's uniquely restrictive environment present strong selection pressures to any metastasizing cells (Fig. 12A, Table 2). Tumor cells circulating through the brain vasculature arrest in the organ at capillary branch points due to their large size, or via interactions between tumor cells and the endothelium [15]. For example, the most commonly upregulated gene in BC cells that have metastasized to the brain compared to other organs is α2,6-sialyltransferase ST6GALNAC5, an enzyme that modifies cell surface receptors and promotes cell adhesion to the brain vasculature [15,252]. Following adhesion to the vasculature, tumor cells express proteases like MMPs and cathepsins to break down the ECM and tight junctions between ECs, respectively, [15,251,253] and soluble factors like VEGF, FGF2, and TNFα to increase permeability of the BBB [15,247,251,253], thereby enabling paracellular extravasation of tumor cells across the endothelium [9].

Upon reaching the brain parenchyma, tumor cells must adapt to a challenging environment of low oxygen tension and limited nutrients [9]. These conditions select for tumor cells that can upregulate glycolysis [15,251]. For example, the most upregulated gene in brain metastatic BC cells compared to primary BC cells is hexokinase-2—an enzyme that converts glucose to glucose-6-phosphate, thereby trapping the nutrient in the cell [254]. Tumor cells that successfully metastasize to the brain also upregulate expression of integrins to facilitate adhesion to the environment [15,251], adopt some characteristics of neurons [15,251], and remodel the vasculature to secure a source of nutrients [9,15,251]. Interestingly, metastatic cells from primary BC and melanoma co-option the existing vasculature, while cells from primary lung and renal cancers promote angiogenesis [9,251]. Finally, metastatic tumor cells must contend with brain-specific astrocyte and microglial immune cell populations. Specifically, tumor-activated astrocytes secrete chemokines like interferon α and TNF that promote tumor cell survival, growth, and chemoresistance [9,15,247]. Microglial cells, on the other hand, typically target and kill tumor cells through TNFα and inducible nitric oxide synthase-mediated mechanisms [9]; hence, reactivation of microglial cells is a potential immunotherapeutic strategy [247]. Brain metastases also recruit MDSCs and T cells [247].

Given the highly selective brain tissue microenvironment, tumor cells of different origins often converge on similar survival mechanisms—including altered metabolism, astrocyte activation, and chemoresistance—once they have metastasized to the brain [15,251]. Notably, the BBB reforms following establishment of a metastatic lesion. This remodeled BBB, dubbed the blood-tumor barrier (BTB), features activated immune cells and higher permeability; however, it remains impermeable to most chemotherapies and presents a significant challenge to the delivery of other molecular and cellular therapies [9,15].

Microfluidic Models of Brain Metastases. Microphysiological models of the healthy BBB (reviewed in [248,255]) can recreate the tight junctions, nutrient transporter expression, impermeability, and perfusion of the vasculature; mimic the nutrient-restricted brain parenchyma; and incorporate astrocytes and/or microglial cells. These models have been used to characterize organ-specific molecular and cellular mechanisms and drug transport across the BBB. The majority of these platforms consist of EC-lined microfluidic channels where the EC cells are either brain-specific or treated with all-trans retinoic acid for 2–3 days, a method that temporarily tightens the BBB [256]. A 2020 report self-assembled a BBB vasculature from brain-specific ECs, pericytes, and astrocytes [257]. It should be noted that several studies have been published using BBB EC generated directly from iPSC without an intervening mesoderm induction—these cells have now been shown definitively to be epithelial and not endothelial cells [258].

Recent work capitalizes on the strengths of healthy BBB platforms to model metastasis to the brain [212,213,259–264]. For example, a 2016 study separated a fluid-filled vascular chamber from a gel-filled brain parenchyma with an ECM barrier coated with brain microvascular ECs on one side and astrocytes on the other; inclusion of flow in the vascular chamber and astrocytes were critical to BBB integrity. Lung cancer, BC, and melanoma cells lines—but not liver cancer or primary brain cancer cell lines—in the vascular chamber extravasated into the brain parenchyma and disrupted the integrity of the BBB, mimicking *in vivo* metastatic patterns [259]. A 2019 report coupled a lung TME to a brain microenvironment and examined metastasis of NSCLC to the brain (Fig. 12B). In this platform, metastasizing NSCLC cells had to intravasate into the circulation, travel to the brain compartment, extravasate across the BBB, and establish themselves in the brain

parenchyma. This model can characterize the metastatic capacity of different cell lines, and the study showed that metastasis of NSCLC cell lines increases with expression of the protein aldo–keto reductase family 1 B10 [260]. Additional models mimic the *in vivo* transition from the BBB to the BTB through addition of cancer cells [259,261,262] or inflammatory cytokines [263] to otherwise healthy BBB microfluidic platforms. These BTB models expressed fewer tight junctions and transporters, were more permeable, and demonstrated higher rates of extravasation. Finally, Oliver et al. [264] used a BBB microfluidic model to characterize the phenotype of metastatic and non-metastatic BC cell lines and patient-derived cells, which may facilitate clinical predictions of metastatic risk through analysis of CTCs.

Future Directions. Future BBB and BTB microfluidic models should seek to replace EC-lined microfluidic channels with self-assembled vasculature models, which more accurately mimic the architecture of native vessels. This is especially pertinent since vessel branching and density are known factors in brain metastasis. Multiple current microfluidic models couple primary TMEs to brain models, and continued efforts to improve the physiological relevance of both microenvironments and the fluidic connections may produce valuable insights into metastasis to the brain—including comprehensive characterization of the process by tumor of origin. Inclusion of hypoxia and microglial cells will also improve the relevance of future brain metastasis microfluidic models.

4. Conclusions & Future Directions

Tissue engineered microfluidic platforms have vastly improved the organ-specificity of current physiological and pathological preclinical model systems. These devices can incorporate organ-specific architecture, cell types, vessel structures, and physiochemical features (i.e., cyclic mechanical strain, interstitial pressure, hypoxia, ECM composition). Further, recent work demonstrates that these systems accurately recapitulate native biology. As reviewed here, this emerging technology can be employed to study the organ-specific TME, an effort that has provided valuable insights on the immunobiology of carcinogenesis and metastasis and the utility of various chemo- and immuno-therapies.

However, the building blocks of most current tumor-on-chip models are immortalized cell lines, which cannot reproduce certain biological phenomena and are unrealistically homogeneous. Future work should seek to incorporate autologous cell sources, which may include primary cells and/or induced pluripotent stem cells. Organoids, which recapitulate many features of whole organ physiology, and immune cells, now known to play a key role in tumor development and progression, may also improve the relevance of current tumor-on-chip models. Additionally, different cell types (i.e., ECs, CAFs, tumor cells, immune cells, and/or organ-specific specialized cell types) should be introduced at physiologically-relevant ratios. These autologous, proportionally accurate tumor-on-chip systems may elucidate unknown principles of tumor immunobiology and enable patient-specific assessments of response to therapy. Further, long-range interactions between organs are a recognized principle of carcinogenesis and metastasis. Future microfluidic platforms should capitalize on the modular nature of microfluidic technology to connect the organs involved in cancer—that is, the primary tumor, the metastatic niche, and tissues of the immune system—via fluidic lines that mimic circulation throughout the body.

Declaration of Competing Interest

The authors declare the following financial interests/personal relationships which may be considered as potential competing interests: CCWH and SCG are co-founders and CCWH is the CSO of Aracari Biosciences, a company that is commercializing organ-on-chip technology through a patent licensing agreement with UCI. The terms of this arrangement are approved and monitored by the Conflict of Interest Committee at UCI (CCWH) and UC Davis (SCG). The remaining authors (NDP, VSS, YB, SPG, SG, RCF) have no declarations of interest.

Acknowledgements

The graphical abstract, Fig. 1, Fig. 2, and panel A of Figs. 3–12 were created using Biorender.com.

This work is supported by the National Institutes of Health [R21 CA223836 (RCF), UG3/UH3 HL141800 (SCG), UG3DK122639 (CCWH, SCG), UG3/UH3 TR002137 (CCWH), R61HL15430701 (CCWH), U54 CA217378 (CCWH)]; and the University of California System's Cancer Research Coordinating Committee [C21CR2153 (SCG)].

References

[1] H. Sung, J. Ferlay, R.L. Siegel, M. Laversanne, I. Soerjomataram, A. Jemal, F. Bray, Global cancer statistics 2020: GLOBOCAN estimates of incidence and mortality worldwide for 36 cancers in 185 countries, CA Cancer J Clin, (2021).
[2] Cancer, World Health Organization, 2018.
[3] R.L. Siegel, K.D. Miller, A. Jemal, Cancer statistics, 2018, CA: A Cancer Journal for Clinicians, 68 (2018) 7-30.
[4] A.C. Society, Global Cancer Facts & Figures 4th Edition, in: A.C. Society (Ed.), American Cancer Society, 2018.
[5] D. Hanahan, R.A. Weinberg, Hallmarks of cancer: the next generation, Cell 144 (2011) 646–674.
[6] D. Hanahan, R.A. Weinberg, The hallmarks of cancer, Cell 100 (2000) 57–70.
[7] A.C. Obenauf, J. Massague, Surviving at a Distance: Organ-Specific Metastasis, Trends Cancer 1 (2015) 76–91.
[8] A. Mielgo, M.C. Schmid, Liver Tropism in Cancer: The Hepatic Metastatic Niche, Cold Spring Harb Perspect Med 10 (2020).
[9] F.J. Lowery, D. Yu, Brain metastasis: Unique challenges and open opportunities, Biochim Biophys Acta Rev Cancer 2017 (1867) 49–57.
[10] A.E. Place, S. Jin Huh, K. Polyak, The microenvironment in breast cancer progression: biology and implications for treatment, Breast Cancer Res 13 (2011) 227.
[11] M. Karlou, V. Tzelepi, E. Efstathiou, Therapeutic targeting of the prostate cancer microenvironment, Nat Rev Urol 7 (2010) 494–509.
[12] N.K. Altorki, G.J. Markowitz, D. Gao, J.L. Port, A. Saxena, B. Stiles, T. McGraw, V. Mittal, The lung microenvironment: an important regulator of tumour growth and metastasis, Nat Rev Cancer 19 (2019) 9–31.
[13] S.I. Grivennikov, F.R. Greten, M. Karin, Immunity, inflammation, and cancer, Cell 140 (2010) 883–899.
[14] K.C. Valkenburg, A.E. de Groot, K.J. Pienta, Targeting the tumour stroma to improve cancer therapy, Nat Rev Clin Oncol 15 (2018) 366–381.
[15] A.S. Achrol, R.C. Rennert, C. Anders, R. Soffietti, M.S. Ahluwalia, L. Nayak, S. Peters, N.D. Arvold, G.R. Harsh, P.S. Steeg, S.D. Chang, Brain metastases, Nat Rev Dis Primers 5 (2019) 5.
[16] S. Paget, THE DISTRIBUTION OF SECONDARY GROWTHS IN CANCER OF THE BREAST, The Lancet 133 (1889) 571–573.
[17] J. Ewing, Neoplastic diseases : a treatise on tumors, W. B. Saunders, Philadelphia; London, 1928.
[18] B.Z. Qian, J.W. Pollard, Macrophage diversity enhances tumor progression and metastasis, Cell 141 (2010) 39–51.
[19] L. Cassetta, J.W. Pollard, Targeting macrophages: therapeutic approaches in cancer, Nat Rev Drug Discov 17 (2018) 887–904.
[20] C.H. Wong, K.W. Siah, A.W. Lo, Estimation of clinical trial success rates and related parameters, Biostatistics 20 (2018) 273–286.
[21] S.J. Hachey, C.C.W. Hughes, Applications of tumor chip technology, Lab Chip 18 (2018) 2893–2912.
[22] P.S. Yoon, N. Del Piccolo, V.S. Shirure, Y. Peng, A. Kirane, R.J. Canter, R.C. Fields, S.C. George, S. Gholami, Advances in Modeling the Immune Microenvironment of Colorectal Cancer, Frontiers in Immunology 11 (2021).
[23] L.A. Low, C. Mummery, B.R. Berridge, C.P. Austin, D.A. Tagle, Organs-on-chips: into the next decade, Nat Rev Drug Discov (2020).
[24] J. Ahn, Y.J. Sei, N.L. Jeon, Y. Kim, Tumor Microenvironment on a Chip: The Progress and Future Perspective, Bioengineering (Basel) 4 (2017).
[25] D. Caballero, S. Kaushik, V.M. Correlo, J.M. Oliveira, R.L. Reis, S.C. Kundu, Organ-on-chip models of cancer metastasis for future personalized medicine: From chip to the patient, Biomaterials 149 (2017) 98–115.
[26] Y.L. Huang, J.E. Segall, M. Wu, Microfluidic modeling of the biophysical microenvironment in tumor cell invasion, Lab Chip 17 (2017) 3221–3233.

[27] H.F. Tsai, A. Trubelja, A.Q. Shen, G. Bao, Tumour-on-a-chip: microfluidic models of tumour morphology, growth and microenvironment, J R Soc Interface 14 (2017).
[28] A. Avendano, M. Cortes-Medina, J.W. Song, Application of 3-D Microfluidic Models for Studying Mass Transport Properties of the Tumor Interstitial Matrix, Front Bioeng Biotechnol 7 (2019) 6.
[29] V. Kumar, S. Varghese, Ex Vivo Tumor-on-a-Chip Platforms to Study Intercellular Interactions within the Tumor Microenvironment, Adv Healthc Mater 8 (2019) e1801198.
[30] M. Shang, R.H. Soon, C.T. Lim, B.L. Khoo, J. Han, Microfluidic modelling of the tumor microenvironment for anti-cancer drug development, Lab Chip 19 (2019) 369–386.
[31] A. Sontheimer-Phelps, B.A. Hassell, D.E. Ingber, Modelling cancer in microfluidic human organs-on-chips, Nat Rev Cancer 19 (2019) 65–81.
[32] G. Trujillo-de Santiago, B.G. Flores-Garza, J.A. Tavares-Negrete, I.M. Lara-Mayorga, I. Gonzalez-Gamboa, Y.S. Zhang, A. Rojas-Martinez, R. Ortiz-Lopez, M.M. Alvarez, The Tumor-on-Chip: Recent Advances in the Development of Microfluidic Systems to Recapitulate the Physiology of Solid Tumors, Materials (Basel), 12 (2019).
[33] L. Wan, C.A. Neumann, P.R. LeDuc, Tumor-on-a-chip for integrating a 3D tumor microenvironment: chemical and mechanical factors, Lab Chip 20 (2020) 873–888.
[34] S.T. Modules, Anatomy of the Lung, National Institutes of Health, National Cancer Institute.
[35] H.H. Aung, A. Sivakumar, S.K. Gholami, S.P. Venkateswaran, B. Gorain, Shadab, Chapter 1 - An Overview of the Anatomy and Physiology of the Lung, in: P. Kesharwani (Ed.) Nanotechnology-Based Targeted Drug Delivery Systems for Lung Cancer, Academic Press2019, pp. 1-20.
[36] K. Suresh, L.A. Shimoda, Lung Circulation, Comprehensive, Physiology (2016) 897–943.
[37] D. Hartl, R. Tirouvanziam, J. Laval, C.M. Greene, D. Habiel, L. Sharma, A.O. Yildirim, C.S. Dela Cruz, C.M. Hogaboam, Innate Immunity of the Lung: From Basic Mechanisms to Translational Medicine, J Innate Immun 10 (2018) 487–501.
[38] H. Lemjabbar-Alaoui, O.U. Hassan, Y.W. Yang, P. Buchanan, Lung cancer: Biology and treatment options, Biochim Biophys Acta 2015 (1856) 189–210.
[39] R.S. Herbst, D. Morgensztern, C. Boshoff, The biology and management of non-small cell lung cancer, Nature 553 (2018) 446–454.
[40] E.E. Graves, A. Maity, Q.T. Le, The tumor microenvironment in non-small-cell lung cancer, Semin Radiat Oncol 20 (2010) 156–163.
[41] M.C. Dieu-Nosjean, M. Antoine, C. Danel, D. Heudes, M. Wislez, V. Poulot, N. Rabbe, L. Laurans, E. Tartour, L. de Chaisemartin, S. Lebecque, W.H. Fridman, J. Cadranel, Long-term survival for patients with non-small-cell lung cancer with intratumoral lymphoid structures, J Clin Oncol 26 (2008) 4410–4417.
[42] M. Gotte, I. Kovalszky, Extracellular matrix functions in lung cancer, Matrix Biol 73 (2018) 105–121.
[43] H.G. Thompson, D.T. Truong, C.K. Griffith, S.C. George, A three-dimensional in vitro model of angiogenesis in the airway mucosa, Pulm Pharmacol Ther 20 (2007) 141–148.
[44] N.K. Malavia, J.D. Mih, C.B. Raub, B.T. Dinh, S.C. George, IL-13 induces a bronchial epithelial phenotype that is profibrotic, Respir Res 9 (2008) 27.
[45] D. Huh, B.D. Matthews, A. Mammoto, M. Montoya-Zavala, H.Y. Hsin, D.E. Ingber, Reconstituting Organ-Level Lung Functions on a Chip, Science 328 (2010) 1662–1668.
[46] K.H. Benam, R. Villenave, C. Lucchesi, A. Varone, C. Hubeau, H.-H. Lee, S.E. Alves, M. Salmon, T.C. Ferrante, J.C. Weaver, A. Bahinski, G.A. Hamilton, D.E. Ingber, Small airway-on-a-chip enables analysis of human lung inflammation and drug responses in vitro, Nature Methods 13 (2016) 151–157.
[47] D. Huh, D.C. Leslie, B.D. Matthews, J.P. Fraser, S. Jurek, G.A. Hamilton, K.S. Thorneloe, M.A. McAlexander, D.E. Ingber, A Human Disease Model of Drug Toxicity-Induced Pulmonary Edema in a Lung-on-a-Chip Microdevice, Science Translational Medicine 4 (2012).
[48] S.M. Ehsan, K.M. Welch-Reardon, M.L. Waterman, C.C. Hughes, S.C. George, A three-dimensional in vitro model of tumor cell intravasation, Integr Biol (Camb) 6 (2014) 603–610.
[49] L. Ying, Z. Zhu, Z. Xu, T. He, E. Li, Z. Guo, F. Liu, C. Jiang, Q. Wang, Cancer Associated Fibroblast-Derived Hepatocyte Growth Factor Inhibits the Paclitaxel-Induced Apoptosis of Lung Cancer A549 Cells by Up-Regulating the PI3K/Akt and GRP78 Signaling on a Microfluidic Platform, PLoS One 10 (2015) e0129593.
[50] A. Zuchowska, E. Jastrzebska, M. Chudy, A. Dybko, Z. Brzozka, 3D lung spheroid cultures for evaluation of photodynamic therapy (PDT) procedures in microfluidic Lab-on-a-Chip system, Anal Chim Acta 990 (2017) 110–120.
[51] S.W. Lee, H.S. Kwak, M.H. Kang, Y.Y. Park, G.S. Jeong, Fibroblast-associated tumour microenvironment induces vascular structure-networked tumouroid, Sci Rep 8 (2018) 2365.
[52] D. Kalinowska, I. Grabowska-Jadach, M. Liwinska, M. Drozd, M. Pietrzak, A. Dybko, Z. Brzozka, Studies on effectiveness of PTT on 3D tumor model under microfluidic conditions using aptamer-modified nanoshells, Biosens Bioelectron 126 (2019) 214–221.
[53] Z. Li, T. Guo, L. Fang, N. Li, X. Wang, P. Wang, S. Zhao, F. Li, Y. Cui, X. Shu, L. Zhao, J. Li, C. Gu, MACC1 overexpression in carcinomaassociated fibroblasts induces the invasion of lung adenocarcinoma cells via paracrine signaling, Int J Oncol 54 (2019) 1367–1375.
[54] V. Mani, Z. Lyu, V. Kumar, B. Ercal, H. Chen, S.V. Malhotra, U. Demirci, Epithelial-to-Mesenchymal Transition (EMT) and Drug Response in Dynamic Bioengineered Lung Cancer Microenvironment, Adv Biosyst 3 (2019) e1800223.
[55] J. Paek, S.E. Park, Q. Lu, K.T. Park, M. Cho, J.M. Oh, K.W. Kwon, Y.S. Yi, J.W. Song, H.I. Edelstein, J. Ishibashi, W. Yang, J.W. Myerson, R.Y. Kiseleva, P. Aprelev, E. D. Hood, D. Stambolian, P. Seale, V.R. Muzykantov, D. Huh, Microphysiological Engineering of Self-Assembled and Perfusable Microvascular Beds for the Production of Vascularized Three-Dimensional Human Microtissues, ACS Nano 13 (2019) 7627–7643.
[56] N. Dhiman, N. Shagaghi, M. Bhave, H. Sumer, P. Kingshott, S.N. Rath, Indirect co-culture of lung carcinoma cells with hyperthermia-treated mesenchymal stem cells influences tumor spheroid growth in a collagen-based 3-dimensional microfluidic model, Cytotherapy (2020).
[57] P.G. Miller, C.Y. Chen, Y.I. Wang, E. Gao, M.L. Shuler, Multiorgan microfluidic platform with breathable lung chamber for inhalation or intravenous drug screening and development, Biotechnol Bioeng 117 (2020) 486–497.
[58] B.A. Hassell, G. Goyal, E. Lee, A. Sontheimer-Phelps, O. Levy, C.S. Chen, D.E. Ingber, Human Organ Chip Models Recapitulate Orthotopic Lung Cancer Growth, Therapeutic Responses, and Tumor Dormancy In Vitro, Cell Rep 21 (2017) 508–516.
[59] J. Song, Y. Zhang, C. Zhang, X. Du, Z. Guo, Y. Kuang, Y. Wang, P. Wu, K. Zou, L. Zou, J. Lv, Q. Wang, A microfluidic device for studying chemotaxis mechanism of bacterial cancer targeting, Sci Rep 8 (2018) 6394.
[60] A.L. Beckwith, L.F. Velasquez-Garcia, J.T. Borenstein, Microfluidic Model for Evaluation of Immune Checkpoint Inhibitors in Human Tumors, Adv Healthc Mater 8 (2019) e1900289.
[61] N. Moore, D. Doty, M. Zielstorff, I. Kariv, L.Y. Moy, A. Gimbel, J.R. Chevillet, N. Lowry, J. Santos, V. Mott, L. Kratchman, T. Lau, G. Addona, H. Chen, J.T. Borenstein, A multiplexed microfluidic system for evaluation of dynamics of immune-tumor interactions, Lab Chip 18 (2018) 1844–1858.
[62] SEER Training Modules, Breast Cancer, National Institutes of Health, National Cancer Institute.
[63] R.A. Jesinger, Breast anatomy for the interventionalist, Tech Vasc Interv Radiol 17 (2014) 3–9.
[64] M.M. Morgan, L.A. Schuler, J.C. Ciciliano, B.P. Johnson, E.T. Alarid, D.J. Beebe, Modeling chemical effects on breast cancer: the importance of the microenvironment in vitro, Integr Biol (Camb) 12 (2020) 21–33.
[65] A.C. Society, Breast Cancer Facts & Figures 2019-20., in: A.C. Society (Ed.) Atlanta, 2020.
[66] H. Yu, J.K. Mouw, V.M. Weaver, Forcing form and function: biomechanical regulation of tumor evolution, Trends Cell Biol 21 (2011) 47–56.
[67] M.J. Paszek, V.M. Weaver, The tension mounts: mechanics meets morphogenesis and malignancy, J Mammary Gland Biol Neoplasia 9 (2004) 325–342.
[68] M.W. Conklin, J.C. Eickhoff, K.M. Riching, C.A. Pehlke, K.W. Eliceiri, P.P. Provenzano, A. Friedl, P.J. Keely, Aligned collagen is a prognostic signature for survival in human breast carcinoma, Am J Pathol 178 (2011) 1221–1232.
[69] G.L. Semenza, The hypoxic tumor microenvironment: A driving force for breast cancer progression, Biochim Biophys Acta 2016 (1863) 382–391.
[70] Y. Choi, E. Hyun, J. Seo, C. Blundell, H.C. Kim, E. Lee, S.H. Lee, A. Moon, W.K. Moon, D. Huh, A microengineered pathophysiological model of early-stage breast cancer, Lab on a Chip 15 (2015) 3350–3357.
[71] L.L. Bischel, D.J. Beebe, K.E. Sung, Microfluidic model of ductal carcinoma in situ with 3D, organotypic structure, BMC Cancer 15 (2015) 12.
[72] J.M. Ayuso, A. Gillette, K. Lugo-Cintrón, S. Acevedo-Acevedo, I. Gomez, M. Morgan, T. Heaster, K.B. Wisinski, S.P. Palecek, M.C. Skala, D.J. Beebe, Organotypic microfluidic breast cancer model reveals starvation-induced spatial-temporal metabolic adaptations, EBioMedicine 37 (2018) 144–157.
[73] I.K. Zervantonakis, S.K. Hughes-Alford, J.L. Charest, J.S. Condeelis, F.B. Gertler, R.D. Kamm, Three-dimensional microfluidic model for tumor cell intravasation and endothelial barrier function, Proc Natl Acad Sci U S A 109 (2012) 13515–13520.
[74] D. Devadas, T.A. Moore, N. Walji, E.W.K. Young, A microfluidic mammary gland coculture model using parallel 3D lumens for studying epithelial-endothelial migration in breast cancer, Biomicrofluidics 13 (2019) 064122.
[75] V.S. Shirure, Y. Bi, M.B. Curtis, A. Lezia, M.M. Goedegebuure, S.P. Goedegebuure, R. Aft, R.C. Fields, S.C. George, Tumor-on-a-chip platform to investigate progression and drug sensitivity in cell lines and patient-derived organoids, Lab on a Chip 18 (2018) 3687–3702.
[76] A. Sobrino, D.T. Phan, R. Datta, X. Wang, S.J. Hachey, M. Romero-Lopez, E. Gratton, A.P. Lee, S.C. George, C.C. Hughes, 3D microtumors in vitro supported by perfused vascular networks, Sci Rep 6 (2016) 31589.
[77] J.M. Ayuso, R. Truttschel, M.M. Gong, M. Humayun, M. Virumbrales-Munoz, R. Vitek, M. Felder, S.D. Gillies, P. Sondel, K.B. Wisinski, M. Patankar, D.J. Beebe, M.C. Skala, Evaluating natural killer cell cytotoxicity against solid tumors using a microfluidic model, OncoImmunology 8 (2019) 1553477.
[78] V.S. Shirure, S.F. Lam, B. Shergill, Y.E. Chu, N.R. Ng, S.C. George, Quantitative design strategies for fine control of oxygen in microfluidic systems, Lab Chip 20 (2020) 3036–3050.
[79] S.F. Lam, V.S. Shirure, Y.E. Chu, A.G. Soetikno, S.C. George, Microfluidic device to attain high spatial and temporal control of oxygen, PLoS One 13 (2018) e0209574.
[80] M.M. Morgan, L.M. Arendt, E.T. Alarid, D.J. Beebe, B.P. Johnson, Mammary adipose stromal cells derived from obese women reduce sensitivity to the aromatase inhibitor anastrazole in an organotypic breast model, FASEB J 33 (2019) 8623–8633.

[81] M.M. Morgan, M.K. Livingston, J.W. Warrick, E.M. Stanek, E.T. Alarid, D.J. Beebe, B.P. Johnson, Mammary fibroblasts reduce apoptosis and speed estrogen-induced hyperplasia in an organotypic MCF7-derived duct model, Sci Rep 8 (2018) 7139.
[82] D.D. Truong, A. Kratz, J.G. Park, E.S. Barrientos, H. Saini, T. Nguyen, B. Pockaj, G. Mouneimne, J. LaBaer, M. Nikkhah, A Human Organotypic Microfluidic Tumor Model Permits Investigation of the Interplay between Patient-Derived Fibroblasts and Breast Cancer Cells, Cancer Res 79 (2019) 3139–3151.
[83] D. Truong, J. Puleo, A. Llave, G. Mouneimne, R.D. Kamm, M. Nikkhah, Breast Cancer Cell Invasion into a Three Dimensional Tumor-Stroma Microenvironment, Sci Rep 6 (2016) 34094.
[84] J.E. McNeal, Normal histology of the prostate, Am J Surg Pathol 12 (1988) 619–633.
[85] C. Abate-Shen, M.M. Shen, Molecular genetics of prostate cancer, Genes Dev 14 (2000) 2410–2434.
[86] O. Singh, S.R. Bolla, Anatomy, Abdomen and Pelvis, Prostate, StatPearls, Treasure Island (FL), 2020.
[87] N. Vitkin, S. Nersesian, D.R. Siemens, M. Koti, The Tumor Immune Contexture of Prostate Cancer, Front Immunol 10 (2019) 603.
[88] Q. Feng, B. He, Androgen Receptor Signaling in the Development of Castration-Resistant Prostate Cancer, Front Oncol 9 (2019) 858.
[89] M.H. Tan, J. Li, H.E. Xu, K. Melcher, E.L. Yong, Androgen receptor: structure, role in prostate cancer and drug discovery, Acta Pharmacol Sin 36 (2015) 3–23.
[90] C. Levesque, P.S. Nelson, Cellular Constituents of the Prostate Stroma: Key Contributors to Prostate Cancer Progression and Therapy Resistance, Cold Spring Harb Perspect Med 8 (2018).
[91] P. Chiarugi, P. Paoli, P. Cirri, Tumor microenvironment and metabolism in prostate cancer, Semin Oncol 41 (2014) 267–280.
[92] J.A. Tuxhorn, G.E. Ayala, M.J. Smith, V.C. Smith, T.D. Dang, D.R. Rowley, Reactive stroma in human prostate cancer: induction of myofibroblast phenotype and extracellular matrix remodeling, Clin Cancer Res 8 (2002) 2912–2923.
[93] L. Jiang, F. Ivich, S. Tahsin, M. Tran, S.B. Frank, C.K. Miranti, Y. Zohar, Human stroma and epithelium co-culture in a microfluidic model of a human prostate gland, Biomicrofluidics 13 (2019) 064116.
[94] M. Domenech, R. Bjerregaard, W. Bushman, D.J. Beebe, Hedgehog signaling in myofibroblasts directly promotes prostate tumor cell growth, Integr Biol (Camb) 4 (2012) 142–152.
[95] S.C. Kerr, M.M. Morgan, A.A. Gillette, M.K. Livingston, K.M. Lugo-Cintron, P.F. Favreau, L. Florek, B.P. Johnson, J.M. Lang, M.C. Skala, D.J. Beebe, A bioengineered organotypic prostate model for the study of tumor microenvironment-induced immune cell activation, Integr Biol (Camb) 12 (2020) 250–262.
[96] J. Yu, E. Berthier, A. Craig, T.E. de Groot, S. Sparks, P.N. Ingram, D.F. Jarrard, W. Huang, D.J. Beebe, A.B. Theberge, Reconfigurable open microfluidics for studying the spatiotemporal dynamics of paracrine signalling, Nat Biomed Eng 3 (2019) 830–841.
[97] H.J. Pandya, K. Dhingra, D. Prabhakar, V. Chandrasekar, S.K. Natarajan, A. S. Vasan, A. Kulkarni, H. Shafiee, A microfluidic platform for drug screening in a 3D cancer microenvironment, Biosens Bioelectron 94 (2017) 632–642.
[98] K.C. Lin, G. Torga, Y. Sun, R. Axelrod, K.J. Pienta, J.C. Sturm, R.H. Austin, The role of heterogeneous environment and docetaxel gradient in the emergence of polyploid, mesenchymal and resistant prostate cancer cells, Clin Exp Metastasis 36 (2019) 97–108.
[99] T. Tanaka, Colorectal carcinogenesis: Review of human and experimental animal studies, J Carcinog 8 (2009) 5.
[100] S.S. Azzouz LL, Physiology, Large Intestine, In: StatPearls Publishing, Treasure Island (FL), 2020.
[101] SEER Training Modules, Colorectal Cancer, U.S. National Institutes of Health, National Cancer Institute.
[102] A. Bein, W. Shin, S. Jalili-Firoozinezhad, M.H. Park, A. Sontheimer-Phelps, A. Tovaglieri, A. Chalkiadaki, H.J. Kim, D.E. Ingber, Microfluidic Organ-on-a-Chip Models of Human Intestine, Cell Mol Gastroenterol Hepatol 5 (2018) 659–668.
[103] N. Cancer Genome Atlas, Comprehensive molecular characterization of human colon and rectal cancer, Nature, 487 (2012) 330-337.
[104] A. Zeuner, M. Todaro, G. Stassi, R. De Maria, Colorectal cancer stem cells: from the crypt to the clinic, Cell Stem Cell 15 (2014) 692–705.
[105] E. Dekker, P.J. Tanis, J.L.A. Vleugels, P.M. Kasi, M.B. Wallace, Colorectal cancer, Lancet 394 (2019) 1467–1480.
[106] E.J. Kuipers, W.M. Grady, D. Lieberman, T. Seufferlein, J.J. Sung, P.G. Boelens, C. J. van de Velde, T. Watanabe, Colorectal cancer, Nat Rev Dis Primers 1 (2015) 15065.
[107] K. Simon, Colorectal cancer development and advances in screening, Clin Interv Aging 11 (2016) 967–976.
[108] C.R. Boland, A. Goel, Microsatellite instability in colorectal cancer, Gastroenterology 138 (2010) 2073–2087 e2073.
[109] J.L. Markman, S.L. Shiao, Impact of the immune system and immunotherapy in colorectal cancer, J Gastrointest Oncol 6 (2015) 208–223.
[110] J. Galon, A. Costes, F. Sanchez-Cabo, A. Kirilovsky, B. Mlecnik, C. Lagorce-Pages, M. Tosolini, M. Camus, A. Berger, P. Wind, F. Zinzindohoue, P. Bruneval, P.H. Cugnenc, Z. Trajanoski, W.H. Fridman, F. Pages, Type, density, and location of immune cells within human colorectal tumors predict clinical outcome, Science 313 (2006) 1960–1964.
[111] F. Pages, B. Mlecnik, F. Marliot, G. Bindea, F.S. Ou, C. Bifulco, A. Lugli, I. Zlobec, T.T. Rau, M.D. Berger, I.D. Nagtegaal, E. Vink-Borger, A. Hartmann, C. Geppert, J. Kolwelter, S. Merkel, R. Grutzmann, M. Van den Eynde, A. Jouret-Mourin, A. Kartheuser, D. Leonard, C. Remue, J.Y. Wang, P. Bavi, M.H.A. Roehrl, P.S. Ohashi, L.T. Nguyen, S. Han, H.L. MacGregor, S. Hafezi-Bakhtiari, B.G. Wouters, G.V. Masucci, E.K. Andersson, E. Zavadova, M. Vocka, J. Spacek, L. Petruzelka, B. Konopasek, P. Dundr, H. Skalova, K. Nemejcova, G. Botti, F. Tatangelo, P. Delrio, G. Ciliberto, M. Maio, L. Laghi, F. Grizzi, T. Fredriksen, B. Buttard, M. Angelova, A. Vasaturo, P. Maby, S.E. Church, H.K. Angell, L. Lafontaine, D. Bruni, C. El Sissy, N. Haicheur, A. Kirilovsky, A. Berger, C. Lagorce, J.P. Meyers, C. Paustian, Z. Feng, C. Ballesteros-Merino, J. Dijkstra, C. van de Water, S. van Lent-van Vliet, N. Knijn, A.M. Musina, D.V. Scripcariu, B. Popivanova, M. Xu, T. Fujita, S. Hazama, N. Suzuki, H. Nagano, K. Okuno, T. Torigoe, N. Sato, T. Furuhata, I. Takemasa, K. Itoh, P.S. Patel, H.H. Vora, B. Shah, J.B. Patel, K.N. Rajvik, S.J. Pandya, S.N. Shukla, Y. Wang, G. Zhang, Y. Kawakami, F.M. Marincola, P.A. Ascierto, D.J. Sargent, B.A. Fox, J. Galon, International validation of the consensus Immunoscore for the classification of colon cancer: a prognostic and accuracy study, Lancet 391 (2018) 2128–2139.
[112] Y. Xiao, G.J. Freeman, The microsatellite instable subset of colorectal cancer is a particularly good candidate for checkpoint blockade immunotherapy, Cancer Discov 5 (2015) 16–18.
[113] N. Huyghe, P. Baldin, M. Van den Eynde, Immunotherapy with immune checkpoint inhibitors in colorectal cancer: what is the future beyond deficient mismatch-repair tumours?, Gastroenterol Rep (Oxf) 8 (2020) 11–24.
[114] E. Picard, C.P. Verschoor, G.W. Ma, G. Pawelec, Relationships Between Immune Landscapes Genetic Subtypes and Responses to Immunotherapy in Colorectal Cancer, Front Immunol 11 (2020) 369.
[115] D. Ternes, J. Karta, M. Tsenkova, P. Wilmes, S. Haan, E. Letellier, Microbiome in Colorectal Cancer: How to Get from Meta-omics to Mechanism?: (Trends in Microbiology 28, 401–423; 2020), Trends Microbiol 28 (2020) 698.
[116] A.D. Kostic, D. Gevers, C.S. Pedamallu, M. Michaud, F. Duke, A.M. Earl, A.I. Ojesina, J. Jung, A.J. Bass, J. Tabernero, J. Baselga, C. Liu, R.A. Shivdasani, S. Ogino, B.W. Birren, C. Huttenhower, W.S. Garrett, M. Meyerson, Genomic analysis identifies association of Fusobacterium with colorectal carcinoma, Genome Res 22 (2012) 292–298.
[117] V. Koliaraki, C.K. Pallangyo, F.R. Greten, G. Kollias, Mesenchymal Cells in Colon Cancer, Gastroenterology 152 (2017) 964–979.
[118] T. Colangelo, G. Polcaro, L. Muccillo, G. D'Agostino, V. Rosato, P. Ziccardi, A. Lupo, G. Mazzoccoli, L. Sabatino, V. Colantuoni, Friend or foe? The tumour microenvironment dilemma in colorectal cancer, Biochim Biophys Acta Rev Cancer 2017 (1867) 1–18.
[119] L. Vermeulen, E.M.F. De Sousa, M. van der Heijden, K. Cameron, J.H. de Jong, T. Borovski, J.B. Tuynman, M. Todaro, C. Merz, H. Rodermond, M.R. Sprick, K. Kemper, D.J. Richel, G. Stassi, J.P. Medema, Wnt activity defines colon cancer stem cells and is regulated by the microenvironment, Nat Cell Biol 12 (2010) 468–476.
[120] J. Tommelein, L. Verset, T. Boterberg, P. Demetter, M. Bracke, O. De Wever, Cancer-associated fibroblasts connect metastasis-promoting communication in colorectal cancer, Front Oncol 5 (2015) 63.
[121] C. Liu, H. Pei, F. Tan, Matrix Stiffness and Colorectal Cancer, Onco Targets Ther 13 (2020) 2747–2755.
[122] L.H. Katz, M. Likhter, W. Jogunoori, M. Belkin, K. Ohshiro, L. Mishra, TGF-beta signaling in liver and gastrointestinal cancers, Cancer Lett 379 (2016) 166–172.
[123] Y. Hao, D. Baker, P. Ten Dijke, TGF-beta-Mediated Epithelial-Mesenchymal Transition and Cancer Metastasis, Int J Mol Sci 20 (2019).
[124] Y. Itatani, K. Kawada, Y. Sakai, Transforming Growth Factor-beta Signaling Pathway in Colorectal Cancer and Its Tumor Microenvironment, Int J Mol Sci 20 (2019).
[125] T. Vu, P.K. Datta, Regulation of EMT in Colorectal Cancer: A Culprit in Metastasis, Cancers (Basel) 9 (2017).
[126] L.T.H. Phi, I.N. Sari, Y.G. Yang, S.H. Lee, N. Jun, K.S. Kim, Y.K. Lee, H.Y. Kwon, Cancer Stem Cells (CSCs) in Drug Resistance and their Therapeutic Implications in Cancer Treatment, Stem Cells Int 2018 (2018) 5416923.
[127] H.J. Kim, D. Huh, G. Hamilton, D.E. Ingber, Human gut-on-a-chip inhabited by microbial flora that experiences intestinal peristalsis-like motions and flow, Lab Chip 12 (2012) 2165–2174.
[128] P. Shah, J.V. Fritz, E. Glaab, M.S. Desai, K. Greenhalgh, A. Frachet, M. Niegowska, M. Estes, C. Jager, C. Seguin-Devaux, F. Zenhausern, P. Wilmes, A microfluidics-based in vitro model of the gastrointestinal human-microbe interface, Nat Commun 7 (2016) 11535.
[129] S. Jalili-Firoozinezhad, F.S. Gazzaniga, E.L. Calamari, D.M. Camacho, C.W. Fadel, A. Bein, B. Swenor, B. Nestor, M.J. Cronce, A. Tovaglieri, O. Levy, K.E. Gregory, D.T. Breault, J.M.S. Cabral, D.L. Kasper, R. Novak, D.E. Ingber, A complex human gut microbiome cultured in an anaerobic intestine-on-a-chip, Nat Biomed Eng 3 (2019) 520–531.
[130] Y. Wang, D.B. Gunasekara, M.I. Reed, M. DiSalvo, S.J. Bultman, C.E. Sims, S.T. Magness, N.L. Allbritton, A microengineered collagen scaffold for generating a polarized crypt-villus architecture of human small intestinal epithelium, Biomaterials 128 (2017) 44–55.
[131] K.M. Seiler, A. Bajinting, D.M. Alvarado, M.A. Traore, M.M. Binkley, W.H. Goo, W.E. Lanik, J. Ou, U. Ismail, M. Iticovici, C.R. King, K.L. VanDussen, E.A. Swietlicki, V. Gazit, J. Guo, C.J. Luke, T. Stappenbeck, M.A. Ciorba, S.C. George, J.M. Meacham, D.C. Rubin, M. Good, B.W. Warner, Patient-derived small intestinal myofibroblasts direct perfused, physiologically responsive

capillary development in a microfluidic Gut-on-a-Chip Model, Sci Rep 10 (2020) 3842.
[132] M.R. Carvalho, D. Barata, L.M. Teixeira, S. Giselbrecht, R.L. Reis, J.M. Oliveira, R. Truckenmuller, P. Habibovic, Colorectal tumor-on-a-chip system: A 3D tool for precision onco-nanomedicine, Sci Adv 5 (2019) eaaw1317.
[133] M. Chung, J. Ahn, K. Son, S. Kim, N.L. Jeon, Biomimetic Model of Tumor Microenvironment on Microfluidic Platform, Adv Healthc Mater 6 (2017).
[134] J.M. Ayuso, M. Virumbrales-Munoz, A. Lacueva, P.M. Lanuza, E. Checa-Chavarria, P. Botella, E. Fernandez, M. Doblare, S.J. Allison, R.M. Phillips, J. Pardo, L.J. Fernandez, I. Ochoa, Development and characterization of a microfluidic model of the tumour microenvironment, Sci Rep 6 (2016) 36086.
[135] J.M. Ayuso, M. Virumbrales-Munoz, P.H. McMinn, S. Rehman, I. Gomez, M.R. Karim, R. Trusttchel, K.B. Wisinski, D.J. Beebe, M.C. Skala, Tumor-on-a-chip: a microfluidic model to study cell response to environmental gradients, Lab Chip 19 (2019) 3461–3471.
[136] S.Y. Jeong, J.H. Lee, Y. Shin, S. Chung, H.J. Kuh, Co-Culture of Tumor Spheroids and Fibroblasts in a Collagen Matrix-Incorporated Microfluidic Chip Mimics Reciprocal Activation in Solid Tumor Microenvironment, PLoS One 11 (2016) e0159013.
[137] S.J. Hachey, S. Movsesyan, Q.H. Nguyen, G. Burton-Sojo, A. Tankazyan, J. Wu, T. Hoang, D. Zhao, S. Wang, M.M. Hatch, E. Celaya, S. Gomez, G.T. Chen, R.T. Davis, K. Nee, N. Pervolarakis, D.A. Lawson, K. Kessenbrock, A.P. Lee, J. Lowengrub, M.L. Waterman, C.C.W. Hughes, An in vitro vascularized micro-tumor model of human colorectal cancer recapitulates in vivo responses to standard-of-care therapy, Lab Chip 21 (2021) 1333–1351.
[138] S. Parlato, A. De Ninno, R. Molfetta, E. Toschi, D. Salerno, A. Mencattini, G. Romagnoli, A. Fragale, L. Roccazzello, M. Buoncervello, I. Canini, E. Bentivegna, M. Falchi, F.R. Bertani, A. Gerardino, E. Martinelli, C. Natale, R. Paolini, L. Businaro, L. Gabriele, 3D Microfluidic model for evaluating immunotherapy efficacy by tracking dendritic cell behaviour toward tumor cells, Sci Rep 7 (2017) 1093.
[139] A.R. Aref, M. Campisi, E. Ivanova, A. Portell, D. Larios, B.P. Piel, N. Mathur, C. Zhou, R.V. Coakley, A. Bartels, M. Bowden, Z. Herbert, S. Hill, S. Gilhooley, J. Carter, I. Canadas, T.C. Thai, S. Kitajima, V. Chiono, C.P. Paweletz, D.A. Barbie, R.D. Kamm, R.W. Jenkins, 3D microfluidic ex vivo culture of organotypic tumor spheroids to model immune checkpoint blockade, Lab Chip 18 (2018) 3129–3143.
[140] J. Deng, E.S. Wang, R.W. Jenkins, S. Li, R. Dries, K. Yates, S. Chhabra, W. Huang, H. Liu, A.R. Aref, E. Ivanova, C.P. Paweletz, M. Bowden, C.W. Zhou, G.S. Herter-Sprie, J.A. Sorrentino, J.E. Bisi, P.H. Lizotte, A.A. Merlino, M.M. Quinn, L.E. Bufe, A. Yang, Y. Zhang, H. Zhang, P. Gao, T. Chen, M.E. Cavanaugh, A.J. Rode, E. Haines, P.J. Roberts, J.C. Strum, W.G. Richards, J.H. Lorch, S. Parangi, V. Gunda, G.M. Boland, R. Bueno, S. Palakurthi, G.J. Freeman, J. Ritz, W.N. Haining, N.E. Sharpless, H. Arthanari, G.I. Shapiro, D.A. Barbie, N.S. Gray, K.K. Wong, CDK4/6 Inhibition Augments Antitumor Immunity by Enhancing T-cell Activation, Cancer Discov 8 (2018) 216–233.
[141] R.W. Jenkins, A.R. Aref, P.H. Lizotte, E. Ivanova, S. Stinson, C.W. Zhou, M. Bowden, J. Deng, H. Liu, D. Miao, M.X. He, W. Walker, G. Zhang, T. Tian, C. Cheng, Z. Wei, S. Palakurthi, M. Bittinger, H. Vitzthum, J.W. Kim, A. Merlino, M. Quinn, C. Venkataramani, J.A. Kaplan, A. Portell, P.C. Gokhale, B. Phillips, A. Smart, A. Rotem, R.E. Jones, L. Keogh, M. Anguiano, L. Stapleton, Z. Jia, M. Barzily-Rokni, I. Canadas, T.C. Thai, M.R. Hammond, R. Vlahos, E.S. Wang, H. Zhang, S. Li, G.J. Hanna, W. Huang, M.P. Hoang, A. Piris, J.P. Eliane, A.O. Stemmer-Rachamimov, L. Cameron, M.J. Su, P. Shah, B. Izar, M. Thakuria, N.R. LeBoeuf, G. Rabinowits, V. Gunda, S. Parangi, J.M. Cleary, B.C. Miller, S. Kitajima, R. Thummalapalli, B. Miao, T.U. Barbie, V. Sivathanu, J. Wong, W.G. Richards, R. Bueno, C.H. Yoon, J. Miret, M. Herlyn, L.A. Garraway, E.M. Van Allen, G.J. Freeman, P.T. Kirschmeier, J.H. Lorch, P.A. Ott, F.S. Hodi, K.T. Flaherty, R.D. Kamm, G.M. Boland, K.K. Wong, D. Dornan, C.P. Paweletz, D.A. Barbie, Ex Vivo Profiling of PD-1 Blockade Using Organotypic Tumor Spheroids, Cancer Discov 8 (2018) 196–215.
[142] Y. Bi, V.S. Shirure, R. Liu, C. Cunningham, L. Ding, J.M. Meacham, S.P. Goedegebuure, S.C. George, R.C. Fields, Tumor-on-a-chip platform to interrogate the role of macrophages in tumor progression, Integr Biol (Camb) 12 (2020) 221–232.
[143] J.H. Sung, C. Kam, M.L. Shuler, A microfluidic device for a pharmacokinetic-pharmacodynamic (PK-PD) model on a chip, Lab Chip 10 (2010) 446–455.
[144] K.C. Weng, Y.K. Kurokawa, B.S. Hajek, J.A. Paladin, V.S. Shirure, S.C. George, Human Induced Pluripotent Stem-Cardiac-Endothelial-Tumor-on-a-Chip to Assess Anticancer Efficacy and Cardiotoxicity, Tissue Eng Part C Methods 26 (2020) 44–55.
[145] K. Greenhalgh, J. Ramiro-Garcia, A. Heinken, P. Ullmann, T. Bintener, M.P. Pacheco, J. Baginska, P. Shah, A. Frachet, R. Halder, J.V. Fritz, T. Sauter, I. Thiele, S. Haan, E. Letellier, P. Wilmes, Integrated In Vitro and In Silico Modeling Delineates the Molecular Effects of a Synbiotic Regimen on Colorectal-Cancer-Derived Cells, Cell Rep 27 (2019) 1621–1632 e1629.
[146] J. Aleman, A. Skardal, A multi-site metastasis-on-a-chip microphysiological system for assessing metastatic preference of cancer cells, Biotechnol Bioeng 116 (2019) 936–944.
[147] A. Skardal, M. Devarasetty, S. Forsythe, A. Atala, S. Soker, A reductionist metastasis-on-a-chip platform for in vitro tumor progression modeling and drug screening, Biotechnol Bioeng 113 (2016) 2020–2032.
[148] SEER Training Modules, Pancreatic & Biliary Cancer, U.S. National Institutes of Health, National Cancer Institute.
[149] E.B. Chang, P.S. Leung, Pancreatic Physiology, in: P.S. Leung (Ed.) The Gastrointestinal System: Gastrointestinal, Nutritional and Hepatobiliary Physiology, Springer Netherlands, Dordrecht, 2014, pp. 87-105.
[150] S.J. Pandol, Anatomy, The Exocrine Pancreas, San Rafael (CA), 2010.
[151] M. Korc, Normal Function of the Endocrine Pancreas, in: V.L.W.G.e. al (Ed.) The Pancreas: Biology, Pathobiology, and Disease, New York, Raven Press, Ltd, 1993, pp. 751-758.
[152] A.C. Society, What Is Pancreatic Cancer?, American Cancer Society, 2021.
[153] M. Orth, P. Metzger, S. Gerum, J. Mayerle, G. Schneider, C. Belka, M. Schnurr, K. Lauber, Pancreatic ductal adenocarcinoma: biological hallmarks, current status, and future perspectives of combined modality treatment approaches, Radiat Oncol 14 (2019) 141.
[154] K. Young, D.J. Hughes, D. Cunningham, N. Starling, Immunotherapy and pancreatic cancer: unique challenges and potential opportunities, Ther Adv Med Oncol 10 (2018).
[155] A. Adamska, A. Domenichini, M. Falasca, Pancreatic Ductal Adenocarcinoma: Current and Evolving Therapies, Int J Mol Sci 18 (2017).
[156] C. Feig, A. Gopinathan, A. Neesse, D.S. Chan, N. Cook, D.A. Tuveson, The pancreas cancer microenvironment, Clin Cancer Res 18 (2012) 4266–4276.
[157] M. Hidalgo, Pancreatic cancer, N Engl J Med 362 (2010) 1605–1617.
[158] A.H. Morrison, K.T. Byrne, R.H. Vonderheide, Immunotherapy and Prevention of Pancreatic Cancer, Trends Cancer 4 (2018) 418–428.
[159] M. Weniger, K.C. Honselmann, A.S. Liss, The Extracellular Matrix and Pancreatic Cancer: A Complex Relationship, Cancers (Basel) 10 (2018).
[160] D. Thomas, P. Radhakrishnan, Tumor-stromal crosstalk in pancreatic cancer and tissue fibrosis, Mol Cancer 18 (2019) 14.
[161] A.C. Koong, V.K. Mehta, Q.T. Le, G.A. Fisher, D.J. Terris, J.M. Brown, A.J. Bastidas, M. Vierra, Pancreatic tumors show high levels of hypoxia, Int J Radiat Oncol Biol Phys 48 (2000) 919–922.
[162] A.N. Hosein, R.A. Brekken, A. Maitra, Pancreatic cancer stroma: an update on therapeutic targeting strategies, Nat Rev Gastroenterol Hepatol 17 (2020) 487–505.
[163] C. Liang, S. Shi, Q. Meng, D. Liang, S. Ji, B. Zhang, Y. Qin, J. Xu, Q. Ni, X. Yu, Complex roles of the stroma in the intrinsic resistance to gemcitabine in pancreatic cancer: where we are and where we are going, Exp Mol Med 49 (2017) e406.
[164] S. Chen, X. Chen, W. Li, T. Shan, W.R. Lin, J. Ma, X. Cui, W. Yang, G. Cao, Y. Li, L. Wang, Y. Kang, Conversion of epithelial-to-mesenchymal transition to mesenchymal-to-epithelial transition is mediated by oxygen concentration in pancreatic cancer cells, Oncol Lett 15 (2018) 7144–7152.
[165] Y. Ino, R. Yamazaki-Itoh, K. Shimada, M. Iwasaki, T. Kosuge, Y. Kanai, N. Hiraoka, Immune cell infiltration as an indicator of the immune microenvironment of pancreatic cancer, Br J Cancer 108 (2013) 914–923.
[166] D.E. Biancur, A.C. Kimmelman, The plasticity of pancreatic cancer metabolism in tumor progression and therapeutic resistance, Biochim Biophys Acta Rev Cancer 2018 (1870) 67–75.
[167] T.M. Nywening, B.A. Belt, D.R. Cullinan, R.Z. Panni, B.J. Han, D.E. Sanford, R.C. Jacobs, J. Ye, A.A. Patel, W.E. Gillanders, R.C. Fields, D.G. DeNardo, W.G. Hawkins, P. Goedegebuure, D.C. Linehan, Targeting both tumour-associated CXCR2(+) neutrophils and CCR2(+) macrophages disrupts myeloid recruitment and improves chemotherapeutic responses in pancreatic ductal adenocarcinoma, Gut 67 (2018) 1112–1123.
[168] P. Parente, P. Parcesepe, C. Covelli, N. Olivieri, A. Remo, M. Pancione, T.P. Latiano, P. Graziano, E. Maiello, G. Giordano, Crosstalk between the Tumor Microenvironment and Immune System in Pancreatic Ductal Adenocarcinoma: Potential Targets for New Therapeutic Approaches, Gastroenterol Res Pract 2018 (2018) 7530619.
[169] D. Balli, A.J. Rech, B.Z. Stanger, R.H. Vonderheide, Immune Cytolytic Activity Stratifies Molecular Subsets of Human Pancreatic Cancer, Clin Cancer Res 23 (2017) 3129–3138.
[170] D.T. Nguyen, E. Lee, S. Alimperti, R.J. Norgard, A. Wong, J.J. Lee, J. Eyckmans, B. Z. Stanger, C.S. Chen, A biomimetic pancreatic cancer on-chip reveals endothelial ablation via ALK7 signaling, Sci Adv 5 (2019) eaav6789.
[171] J.H. Lee, S.K. Kim, I.A. Khawar, S.Y. Jeong, S. Chung, H.J. Kuh, Microfluidic co-culture of pancreatic tumor spheroids with stellate cells as a novel 3D model for investigation of stroma-mediated cell motility and drug resistance, J Exp Clin Cancer Res 37 (2018) 4.
[172] B. Kramer, L. Haan, M. Vermeer, T. Olivier, T. Hankemeier, P. Vulto, J. Joore, H. L. Lanz, Interstitial Flow Recapitulates Gemcitabine Chemoresistance in A 3D Microfluidic Pancreatic Ductal Adenocarcinoma Model by Induction of Multidrug Resistance Proteins, Int J Mol Sci 20 (2019).
[173] D. Gioeli, C.J. Snow, M.B. Simmers, S.A. Hoang, R.A. Figler, J.A. Allende, D.G. Roller, J.T. Parsons, J.D. Wulfkuhle, E.F. Petricoin, T.W. Bauer, B.R. Wamhoff, Development of a multicellular pancreatic tumor microenvironment system using patient-derived tumor cells, Lab Chip 19 (2019) 1193–1204.
[174] M.J. Bradney, S.M. Venis, Y. Yang, S.F. Konieczny, B. Han, A Biomimetic Tumor Model of Heterogeneous Invasion in Pancreatic Ductal Adenocarcinoma, Small 16 (2020) e1905500.
[175] H.R. Moon, A. Ozcelikkale, Y. Yang, B.D. Elzey, S.F. Konieczny, B. Han, An engineered pancreatic cancer model with intra-tumoral heterogeneity of driver mutations, Lab Chip 20 (2020) 3720–3732.
[176] C.R. Drifka, K.W. Eliceiri, S.M. Weber, W.J. Kao, A bioengineered heterotypic stroma-cancer microenvironment model to study pancreatic ductal adenocarcinoma, Lab Chip 13 (2013) 3965–3975.
[177] M. Beer, N. Kuppalu, M. Stefanini, H. Becker, I. Schulz, S. Manoli, J. Schuette, C. Schmees, A. Casazza, M. Stelzle, A. Arcangeli, A novel microfluidic 3D

platform for culturing pancreatic ductal adenocarcinoma cells: comparison with in vitro cultures and in vivo xenografts, Sci Rep 7 (2017) 1325.
[178] SEER Training Modulues, Anatomy of the Skin, U.S. National Institutes of Health, National Cancer Institute.
[179] E. Sutterby, P. Thurgood, S. Baratchi, K. Khoshmanesh, E. Pirogova, Microfluidic Skin-on-a-Chip Models: Toward Biomimetic Artificial Skin, Small 16 (2020) e2002515.
[180] M.H. Mohammadi, B. Heidary Araghi, V. Beydaghi, A. Geraili, F. Moradi, P. Jafari, M. Janmaleki, K.P. Valente, M. Akbari, A. Sanati-Nezhad, Skin Diseases Modeling using Combined Tissue Engineering and Microfluidic Technologies, Adv Healthc Mater 5 (2016) 2459–2480.
[181] Skin Cancer, American Cancer Society, 2021.
[182] P.Z. Gruber, PM, Skin Cancer, in: S. Publishing (Ed.) StatPearls, Treasure Island, FL, 2020.
[183] P. Boukamp, Non-melanoma skin cancer: what drives tumor development and progression?, Carcinogenesis 26 (2005) 1657–1667.
[184] J. Villanueva, M. Herlyn, Melanoma and the tumor microenvironment, Curr Oncol Rep 10 (2008) 439–446.
[185] M. Marzagalli, N.D. Ebelt, E.R. Manuel, Unraveling the crosstalk between melanoma and immune cells in the tumor microenvironment, Semin Cancer Biol 59 (2019) 236–250.
[186] F.S. Hodi, S.J. O'Day, D.F. McDermott, R.W. Weber, J.A. Sosman, J.B. Haanen, R. Gonzalez, C. Robert, D. Schadendorf, J.C. Hassel, W. Akerley, A.J. van den Eertwegh, J. Lutzky, P. Lorigan, J.M. Vaubel, G.P. Linette, D. Hogg, C.H. Ottensmeier, C. Lebbe, C. Peschel, I. Quirt, J.I. Clark, J.D. Wolchok, J.S. Weber, J. Tian, M.J. Yellin, G.M. Nichol, A. Hoos, W.J. Urba, Improved survival with ipilimumab in patients with metastatic melanoma, N Engl J Med 363 (2010) 711–723.
[187] C. Robert, G.V. Long, B. Brady, C. Dutriaux, M. Maio, L. Mortier, J.C. Hassel, P. Rutkowski, C. McNeil, E. Kalinka-Warzocha, K.J. Savage, M.M. Hernberg, C. Lebbe, J. Charles, C. Mihalcioiu, V. Chiarion-Sileni, C. Mauch, F. Cognetti, A. Arance, H. Schmidt, D. Schadendorf, H. Gogas, L. Lundgren-Eriksson, C. Horak, B. Sharkey, I.M. Waxman, V. Atkinson, P.A. Ascierto, Nivolumab in previously untreated melanoma without BRAF mutation, N Engl J Med 372 (2015) 320–330.
[188] C. Robert, J. Schachter, G.V. Long, A. Arance, J.J. Grob, L. Mortier, A. Daud, M.S. Carlino, C. McNeil, M. Lotem, J. Larkin, P. Lorigan, B. Neyns, C.U. Blank, O. Hamid, C. Mateus, R. Shapira-Frommer, M. Kosh, H. Zhou, N. Ibrahim, S. Ebbinghaus, A. Ribas, K.-. investigators, Pembrolizumab versus Ipilimumab in Advanced Melanoma, N Engl J Med (2015).
[189] S.A. Rosenberg, J.C. Yang, D.J. Schwartzentruber, P. Hwu, F.M. Marincola, S.L. Topalian, N.P. Restifo, M.E. Dudley, S.L. Schwarz, P.J. Spiess, J.R. Wunderlich, M.R. Parkhurst, Y. Kawakami, C.A. Seipp, J.H. Einhorn, D.E. White, Immunologic and therapeutic evaluation of a synthetic peptide vaccine for the treatment of patients with metastatic melanoma, Nat Med 4 (1998) 321–327.
[190] M.A. Postow, J. Chesney, A.C. Pavlick, C. Robert, K. Grossmann, D. McDermott, G.P. Linette, N. Meyer, J.K. Giguere, S.S. Agarwala, M. Shaheen, M.S. Ernstoff, D. Minor, A.K. Salama, M. Taylor, P.A. Ott, L.M. Rollin, C. Horak, P. Gagnier, J.D. Wolchok, F.S. Hodi, Nivolumab and Ipilimumab versus Ipilimumab in Untreated Melanoma, N Engl J Med (2015).
[191] Press release: The Nobel Prize in Physiology or Medicine 2018.
[192] H.E. Abaci, K. Gledhill, Z. Guo, A.M. Christiano, M.L. Shuler, Pumpless microfluidic platform for drug testing on human skin equivalents, Lab Chip 15 (2015) 882–888.
[193] B. Atac, I. Wagner, R. Horland, R. Lauster, U. Marx, A.G. Tonevitsky, R.P. Azar, G. Lindner, Skin and hair on-a-chip: in vitro skin models versus ex vivo tissue maintenance with dynamic perfusion, Lab Chip 13 (2013) 3555–3561.
[194] N. Mori, Y. Morimoto, S. Takeuchi, Skin integrated with perfusable vascular channels on a chip, Biomaterials 116 (2017) 48–56.
[195] M. Wufuer, G. Lee, W. Hur, B. Jeon, B.J. Kim, T.H. Choi, S. Lee, Skin-on-a-chip model simulating inflammation, edema and drug-based treatment, Sci Rep 6 (2016) 37471.
[196] H.E. Abaci, Z. Guo, A. Coffman, B. Gillette, W.H. Lee, S.K. Sia, A.M. Christiano, Human Skin Constructs with Spatially Controlled Vasculature Using Primary and iPSC-Derived Endothelial Cells, Adv Healthc Mater 5 (2016) 1800–1807.
[197] J.M. Ayuso, S. Sadangi, M. Lares, S. Rehman, M. Humayun, K.M. Denecke, M.C. Skala, D.J. Beebe, V. Setaluri, Microfluidic model with air-walls reveals fibroblasts and keratinocytes modulate melanoma cell phenotype, migration, and metabolism, Lab Chip (2021).
[198] L. Businaro, A. De Ninno, G. Schiavoni, V. Lucarini, G. Ciasca, A. Gerardino, F. Belardelli, L. Gabriele, F. Mattei, Cross talk between cancer and immune cells: exploring complex dynamics in a microfluidic environment, Lab Chip 13 (2013) 229–239.
[199] D. Patel, Y. Gao, K. Son, C. Siltanen, R.M. Neve, K. Ferrara, A. Revzin, Microfluidic co-cultures with hydrogel-based ligand trap to study paracrine signals giving rise to cancer drug resistance, Lab Chip 15 (2015) 4614–4624.
[200] A. Albanese, A.K. Lam, E.A. Sykes, J.V. Rocheleau, W.C. Chan, Tumour-on-a-chip provides an optical window into nanoparticle tissue transport, Nat Commun 4 (2013) 2718.
[201] S.R. Abdel-Misih, M. Bloomston, Liver anatomy, Surg Clin North Am 90 (2010) 643–653.
[202] P. Nagy, S.S. Thorgeirsson, J.W. Grisham, Organizational Principles of the Liver, The Liver (2020) 1–13.
[203] I.N. Crispe, The liver as a lymphoid organ, Annual review of immunology 27 (2009) 147–163.
[204] E. Nemeth, A.W. Baird, C. O'Farrelly, Microanatomy of the liver immune system, Semin Immunopathol 31 (2009) 333–343.
[205] A.M. Clark, B. Ma, D.L. Taylor, L. Griffith, A. Wells, Liver metastases: Microenvironments and ex-vivo models, Exp Biol Med (Maywood) 241 (2016) 1639–1652.
[206] P. Brodt, Role of the Microenvironment in Liver Metastasis: From Pre- to Prometastatic Niches, Clin Cancer Res 22 (2016) 5971–5982.
[207] L. Boulter, E. Bullock, Z. Mabruk, V.G. Brunton, The fibrotic and immune microenvironments as targetable drivers of metastasis, Br J Cancer 124 (2021) 27–36.
[208] J. Kim, C. Lee, I. Kim, J. Ro, J. Kim, Y. Min, J. Park, V. Sunkara, Y.S. Park, I. Michael, Y.A. Kim, H.J. Lee, Y.K. Cho, Three-Dimensional Human Liver-Chip Emulating Premetastatic Niche Formation by Breast Cancer-Derived Extracellular Vesicles, ACS Nano 14 (2020) 14971–14988.
[209] S.E. Wheeler, A.M. Clark, D.P. Taylor, C.L. Young, V.C. Pillai, D.B. Stolz, R. Venkataramanan, D. Lauffenburger, L. Griffith, A. Wells, Spontaneous dormancy of metastatic breast cancer cells in an all human liver microphysiologic system, Br J Cancer 111 (2014) 2342–2350.
[210] A.M. Clark, S.E. Wheeler, D.P. Taylor, V.C. Pillai, C.L. Young, R. Prantil-Baun, T. Nguyen, D.B. Stolz, J.T. Borenstein, D.A. Lauffenburger, R. Venkataramanan, L. G. Griffith, A. Wells, A microphysiological system model of therapy for liver micrometastases, Exp Biol Med (Maywood) 239 (2014) 1170–1179.
[211] N. Dioufa, A.M. Clark, B. Ma, C.H. Beckwitt, A. Wells, Bi-directional exosome-driven intercommunication between the hepatic niche and cancer cells, Mol Cancer 16 (2017) 172.
[212] J. Kong, Y. Luo, D. Jin, F. An, W. Zhang, L. Liu, J. Li, S. Fang, X. Li, X. Yang, B. Lin, T. Liu, A novel microfluidic model can mimic organ-specific metastasis of circulating tumor cells, Oncotarget 7 (2016) 78421–78432.
[213] Z. Xu, E. Li, Z. Guo, R. Yu, H. Hao, Y. Xu, Z. Sun, X. Li, J. Lyu, Q. Wang, Design and Construction of a Multi-Organ Microfluidic Chip Mimicking the in vivo Microenvironment of Lung Cancer Metastasis, ACS Appl Mater Interfaces 8 (2016) 25840–25847.
[214] Y. Liu, X. Cao, Characteristics and Significance of the Pre-metastatic Niche, Cancer cell 30 (2016) 668–681.
[215] Y. Maru, The lung metastatic niche, J Mol Med (Berl) 93 (2015) 1185–1192.
[216] M. Charan, P. Dravid, M. Cam, B. Setty, R.D. Roberts, P.J. Houghton, H. Cam, Tumor secreted ANGPTL2 facilitates recruitment of neutrophils to the lung to promote lung pre-metastatic niche formation and targeting ANGPTL2 signaling affects metastatic disease, Oncotarget 11 (2020) 510–522.
[217] J. Kong, H. Tian, F. Zhang, Z. Zhang, J. Li, X. Liu, X. Li, J. Liu, X. Li, D. Jin, X. Yang, B. Sun, T. Guo, Y. Luo, Y. Lu, B. Lin, T. Liu, Extracellular vesicles of carcinoma-associated fibroblasts creates a pre-metastatic niche in the lung through activating fibroblasts, Mol Cancer 18 (2019) 175.
[218] Y. Liu, Y. Gu, Y. Han, Q. Zhang, Z. Jiang, X. Zhang, B. Huang, X. Xu, J. Zheng, X. Cao, Tumor Exosomal RNAs Promote Lung Pre-metastatic Niche Formation by Activating Alveolar Epithelial TLR3 to Recruit Neutrophils, Cancer cell 30 (2016) 243–256.
[219] Z. Wang, C. Yang, L. Li, Z. Zhang, J. Pan, K. Su, W. Chen, J. Li, F. Qiu, J. Huang, CD62L(dim) Neutrophils Specifically Migrate to the Lung and Participate in the Formation of the Pre-Metastatic Niche of Breast Cancer, Front Oncol 10 (2020) 540484.
[220] T.L. Mohammed, A. Chowdhry, G.P. Reddy, J.K. Amorosa, K. Brown, D.S. Dyer, M.E. Ginsburg, D.E. Heitkamp, J. Jeudy, J. Kirsch, H. MacMahon, J.A. Parker, J.G. Ravenel, A.G. Saleh, R.D. Shah, I. Expert Panel on Thoracic, ACR Appropriateness Criteria(R) screening for pulmonary metastases, J Thorac Imaging 26 (2011) W1–W3.
[221] J.S. Jeon, I.K. Zervantonakis, S. Chung, R.D. Kamm, J.L. Charest, In vitro model of tumor cell extravasation, PLoS One 8 (2013) e56910.
[222] S. Bersini, J.S. Jeon, G. Dubini, C. Arrigoni, S. Chung, J.L. Charest, M. Moretti, R. D. Kamm, A microfluidic 3D in vitro model for specificity of breast cancer metastasis to bone, Biomaterials 35 (2014) 2454–2461.
[223] H. Lee, W. Park, H. Ryu, N.L. Jeon, A microfluidic platform for quantitative analysis of cancer angiogenesis and intravasation, Biomicrofluidics 8 (2014) 054102.
[224] J.S. Jeon, S. Bersini, M. Gilardi, G. Dubini, J.L. Charest, M. Moretti, R.D. Kamm, Human 3D vascularized organotypic microfluidic assays to study breast cancer cell extravasation, Proc Natl Acad Sci U S A 112 (2015) 214–219.
[225] M.B. Chen, J.A. Whisler, J. Frose, C. Yu, Y. Shin, R.D. Kamm, On-chip human microvasculature assay for visualization and quantification of tumor cell extravasation dynamics, Nature protocols 12 (2017) 865–880.
[226] N. Peela, D. Truong, H. Saini, H. Chu, S. Mashaghi, S.L. Ham, S. Singh, H. Tavana, B. Mosadegh, M. Nikkhah, Advanced biomaterials and microengineering technologies to recapitulate the stepwise process of cancer metastasis, Biomaterials 133 (2017) 176–207.
[227] M.B. Chen, R.D. Kamm, E. Moeendarbary, Engineered Models of Metastasis with Application to Study Cancer Biomechanics, Adv Exp Med Biol 1092 (2018) 189–207.
[228] C. Kuhlbach, S. da Luz, F. Baganz, V.C. Hass, M.M. Mueller, A Microfluidic System for the Investigation of Tumor Cell Extravasation, Bioengineering (Basel) 5 (2018).
[229] A. Boussommier-Calleja, Y. Atiyas, K. Haase, M. Headley, C. Lewis, R.D. Kamm, The effects of monocytes on tumor cell extravasation in a 3D vascularized microfluidic model, Biomaterials 198 (2019) 180–193.
[230] M.R. Reagan, C.J. Rosen, Navigating the bone marrow niche: translational insights and cancer-driven dysfunction, Nat Rev Rheumatol 12 (2016) 154–168.

[231] G.M. Crane, E. Jeffery, S.J. Morrison, Adult haematopoietic stem cell niches, Nat Rev Immunol 17 (2017) 573–590.
[232] S. Kumar, H. Geiger, HSC Niche Biology and HSC Expansion Ex Vivo, Trends Mol Med 23 (2017) 799–819.
[233] G.D. Roodman, Mechanisms of bone metastasis, N Engl J Med 350 (2004) 1655–1664.
[234] J.T. Buijs, G. van der Pluijm, Osteotropic cancers: from primary tumor to bone, Cancer Lett 273 (2009) 177–193.
[235] H.G. Kopp, S.T. Avecilla, A.T. Hooper, S. Rafii, The bone marrow vascular niche: home of HSC differentiation and mobilization, Physiology (Bethesda) 20 (2005) 349–356.
[236] A. Marturano-Kruik, M.M. Nava, K. Yeager, A. Chramiec, L. Hao, S. Robinson, E. Guo, M.T. Raimondi, G. Vunjak-Novakovic, Human bone perivascular niche-on-a-chip for studying metastatic colonization, Proc Natl Acad Sci U S A 115 (2018) 1256–1261.
[237] A. Bruce, R. Evans, R. Mezan, L. Shi, B.S. Moses, K.H. Martin, L.F. Gibson, Y. Yang, Three-Dimensional Microfluidic Tri-Culture Model of the Bone Marrow Microenvironment for Study of Acute Lymphoblastic Leukemia, PLoS One 10 (2015) e0140506.
[238] S. Hao, L. Ha, G. Cheng, Y. Wan, Y. Xia, D.M. Sosnoski, A.M. Mastro, S.Y. Zheng, A Spontaneous 3D Bone-On-a-Chip for Bone Metastasis Study of Breast Cancer Cells, Small 14 (2018) e1702787.
[239] Y.S. Torisawa, T. Mammoto, E. Jiang, A. Jiang, A. Mammoto, A.L. Watters, A. Bahinski, D.E. Ingber, Modeling Hematopoiesis and Responses to Radiation Countermeasures in a Bone Marrow-on-a-Chip, Tissue Eng Part C Methods 22 (2016) 509–515.
[240] Y.S. Torisawa, C.S. Spina, T. Mammoto, A. Mammoto, J.C. Weaver, T. Tat, J.J. Collins, D.E. Ingber, Bone marrow-on-a-chip replicates hematopoietic niche physiology in vitro, Nat Methods 11 (2014) 663–669.
[241] S. Sieber, L. Wirth, N. Cavak, M. Koenigsmark, U. Marx, R. Lauster, M. Rosowski, Bone marrow-on-a-chip: Long-term culture of human haematopoietic stem cells in a three-dimensional microfluidic environment, J Tissue Eng Regen Med 12 (2018) 479–489.
[242] J. Aleman, S.K. George, S. Herberg, M. Devarasetty, C.D. Porada, A. Skardal, G. Almeida-Porada, Deconstructed Microfluidic Bone Marrow On-A-Chip to Study Normal and Malignant Hemopoietic Cell-Niche Interactions, Small 15 (2019) e1902971.
[243] D.B. Chou, V. Frismantas, Y. Milton, R. David, P. Pop-Damkov, D. Ferguson, A. MacDonald, O. Vargel Bolukbasi, C.E. Joyce, L.S. Moreira Teixeira, A. Rech, A. Jiang, E. Calamari, S. Jalili-Firoozinezhad, B.A. Furlong, L.R. O'Sullivan, C.F. Ng, Y. Choe, S. Marquez, K.C. Myers, O.K. Weinberg, R.P. Hasserjian, R. Novak, O. Levy, R. Prantil-Baun, C.D. Novina, A. Shimamura, L. Ewart, D.E. Ingber, On-chip recapitulation of clinical bone marrow toxicities and patient-specific pathophysiology, Nat Biomed Eng 4 (2020) 394–406.
[244] D.E. Glaser, M.B. Curtis, P.A. Sariano, Z.A. Rollins, B.S. Shergill, A. Anand, A.M. Deely, V.S. Shirure, L. Anderson, J.M. Lowen, N.R. Ng, K. Weilbaecher, D.C. Link, S.C. George, Organ-on-a-chip model of vascularized human bone marrow niches, bioRxiv, (2020) 2020.2004.2017.039339.
[245] C. Ma, M.T. Witkowski, J. Harris, I. Dolgalev, S. Sreeram, W. Qian, J. Tong, X. Chen, I. Aifantis, W. Chen, Leukemia-on-a-chip: Dissecting the chemoresistance mechanisms in B cell acute lymphoblastic leukemia bone marrow niche, Sci Adv 6 (2020).
[246] F. Sharifi, O. Yesil-Celiktas, A. Kazan, S. Maharjan, S. Saghazadeh, K. Firoozbakhsh, B. Firoozabadi, Y.S. Zhang, A hepatocellular carcinoma–bone metastasis-on-a-chip model for studying thymoquinone-loaded anticancer nanoparticles, Bio-Design and Manufacturing 3 (2020) 189–202.
[247] H. Doron, T. Pukrop, N. Erez, A Blazing Landscape: Neuroinflammation Shapes Brain Metastasis, Cancer Res 79 (2019) 423–436.
[248] D.T. Phan, R.H.F. Bender, J.W. Andrejecsk, A. Sobrino, S.J. Hachey, S.C. George, C.C. Hughes, Blood-brain barrier-on-a-chip: Microphysiological systems that capture the complexity of the blood-central nervous system interface, Exp Biol Med (Maywood) 242 (2017) 1669–1678.
[249] A. Verkhratsky, M. Nedergaard, L. Hertz, Why are astrocytes important?, Neurochem Res 40 (2015) 389–401.
[250] C.D. Arvanitis, G.B. Ferraro, R.K. Jain, The blood-brain barrier and blood-tumour barrier in brain tumours and metastases, Nat Rev Cancer 20 (2020) 26–41.
[251] P.E. Fecci, C.D. Champion, J. Hoj, C.M. McKernan, C.R. Goodwin, J.P. Kirkpatrick, C.K. Anders, A.M. Pendergast, J.H. Sampson, The Evolving Modern Management of Brain Metastasis, Clin Cancer Res 25 (2019) 6570–6580.
[252] P.D. Bos, X.H. Zhang, C. Nadal, W. Shu, R.R. Gomis, D.X. Nguyen, A.J. Minn, M.J. van de Vijver, W.L. Gerald, J.A. Foekens, J. Massague, Genes that mediate breast cancer metastasis to the brain, Nature 459 (2009) 1005–1009.
[253] H. Liu, Y. Kato, S.A. Erzinger, G.M. Kiriakova, Y. Qian, D. Palmieri, P.S. Steeg, J.E. Price, The role of MMP-1 in breast cancer growth and metastasis to the brain in a xenograft model, BMC Cancer 12 (2012) 583.
[254] D. Palmieri, D. Fitzgerald, S.M. Shreeve, E. Hua, J.L. Bronder, R.J. Weil, S. Davis, A.M. Stark, M.J. Merino, R. Kurek, H.M. Mehdorn, G. Davis, S.M. Steinberg, P.S. Meltzer, K. Aldape, P.S. Steeg, Analyses of resected human brain metastases of breast cancer reveal the association between up-regulation of hexokinase 2 and poor prognosis, Mol Cancer Res 7 (2009) 1438–1445.
[255] K.M. Fabre, L. Delsing, R. Hicks, N. Colclough, D.C. Crowther, L. Ewart, Utilizing microphysiological systems and induced pluripotent stem cells for disease modeling: a case study for blood brain barrier research in a pharmaceutical setting, Adv Drug Deliv Rev 140 (2019) 129–135.
[256] E.S. Lippmann, A. Al-Ahmad, S.M. Azarin, S.P. Palecek, E.V. Shusta, A retinoic acid-enhanced, multicellular human blood-brain barrier model derived from stem cell sources, Sci Rep 4 (2014) 4160.
[257] S. Lee, M. Chung, S.R. Lee, N.L. Jeon, 3D brain angiogenesis model to reconstitute functional human blood-brain barrier in vitro, Biotechnol Bioeng 117 (2020) 748–762.
[258] T.M. Lu, S. Houghton, T. Magdeldin, J.G.B. Duran, A.P. Minotti, A. Snead, A. Sproul, D.T. Nguyen, J. Xiang, H.A. Fine, Z. Rosenwaks, L. Studer, S. Rafii, D. Agalliu, D. Redmond, R. Lis, Pluripotent stem cell-derived epithelium misidentified as brain microvascular endothelium requires ETS factors to acquire vascular fate, Proc Natl Acad Sci U S A 118 (2021).
[259] H. Xu, Z. Li, Y. Yu, S. Sizdahkhani, W.S. Ho, F. Yin, L. Wang, G. Zhu, M. Zhang, L. Jiang, Z. Zhuang, J. Qin, A dynamic in vivo-like organotypic blood-brain barrier model to probe metastatic brain tumors, Sci Rep 6 (2016) 36670.
[260] W. Liu, J. Song, X. Du, Y. Zhou, Y. Li, R. Li, L. Lyu, Y. He, J. Hao, J. Ben, W. Wang, H. Shi, Q. Wang, AKR1B10 (Aldo-keto reductase family 1 B10) promotes brain metastasis of lung cancer cells in a multi-organ microfluidic chip model, Acta Biomater 91 (2019) 195–208.
[261] T.B. Terrell-Hall, A.G. Ammer, J.I. Griffith, P.R. Lockman, Permeability across a novel microfluidic blood-tumor barrier model, Fluids Barriers CNS 14 (2017) 3.
[262] T.B. Terrell-Hall, M.I. Nounou, F. El-Amrawy, J.I.G. Griffith, P.R. Lockman, Trastuzumab distribution in an in-vivo and in-vitro model of brain metastases of breast cancer, Oncotarget 8 (2017) 83734–83744.
[263] H. Xu, Z. Li, Y. Guo, X. Peng, J. Qin, Probing the response of lung tumor cells to inflammatory microvascular endothelial cells on fluidic microdevice, Electrophoresis 38 (2017) 311–319.
[264] C.R. Oliver, M.A. Altemus, T.M. Westerhof, H. Cheriyan, X. Cheng, M. Dziubinski, Z. Wu, J. Yates, A. Morikawa, J. Heth, M.G. Castro, B.M. Leung, S. Takayama, S.D. Merajver, A platform for artificial intelligence based identification of the extravasation potential of cancer cells into the brain metastatic niche, Lab Chip 19 (2019) 1162–1173.